Gondwana Research 21 (2012) 266–280

Contents lists available at ScienceDirect

Gondwana Research

journal homepage: www.elsevier.com/locate/gr

Neoproterozoic subducted materials in the generation of Mesozoic Luzong volcanic rocks: Evidence from apatite geochemistry and Hf–Nd isotopic decoupling

Ming Tang [a], Xiao-Lei Wang [a,1], Xi-Sheng Xu [a,*], Cheng Zhu [b], Tao Cheng [a], Yao Yu [a]

[a] State Key Laboratory for Mineral Deposits Research, Department of Earth Sciences, Nanjing University, Nanjing, 210093, China
[b] Department of Earth Sciences, Nanjing University, Nanjing, 210093, China

ARTICLE INFO

Article history:
Received 7 October 2010
Received in revised form 23 April 2011
Accepted 10 May 2011
Available online 30 May 2011

Handling Editor: M. Santosh

Keywords:
Apatite
Cl–K decoupling
Zircon effect
Subduction
Luzong volcanic rocks

ABSTRACT

A combined study including apatite geochemistry, zircon U–Pb, Lu–Hf isotopes and whole-rock geochemistry including Nd isotopes was carried out for the late Mesozoic volcanic rocks from the Luzong Basin, in the lower Yangtze River region, South China. Whole-rock geochemistry indicates the enrichments of large ion lithophile elements (LILE) and light rare earth elements (LREE) as well as depletions of Nb, Ta and Ti. The extremely low Cl contents in apatites strongly contrast with the rather high-K contents in whole rocks. Potential loss of Cl during syn- and post-magmatic processes having been ruled out, Cl–K decoupling is attributed to be a feature inherited from the primary magma, which indicates the involvement of highly dehydrated sediments and altered oceanic crust in the mantle source. A calculation based on apatite and whole-rock geochemistry further illustrates that the source was composed of four end-members in the perspective of Cl/K, Cl/Nb and F/K ratios. The Hf–Nd isotopes are decoupled for the basaltic trachytes from the lower volcanic sequences in the Luzong Basin, with rather low $\varepsilon_{Hf}(t)$ values (mean = −10.3) and inconsistent Hf–Nd model ages (Hf ~ 1.8 Ga, Nd ~ 1.3 Ga), which indicate the "zircon effect" that in turn requires the incorporation of continental detritus in the source via subduction. However, Hf and Nd isotopes are nearly coupled for the rocks from the upper volcanic sequences in the Luzong Basin. Late-Mesoproterozoic two-stage Hf and Nd model ages (ca. 1.2 Ga) of rocks from the upper volcanic sequences in the Luzong Basin are similar to those of the Neoproterozoic igneous rocks from the Jiangnan orogen, suggesting their relationship with the same subduction event. Based on the combined apatite geochemistry and Hf–Nd isotopes, this work suggests that the source of Luzong volcanic rocks might incorporate Neoproterozoic subducted slab fragments and detrital sediments that had been blocked in the deep lithospheric mantle below the Luzong area since the Neoproterozoic assembly between the Yangtze and Cathaysia blocks. The partial melting may be triggered by the back-arc lithospheric extension related to the subduction of Paleo-Pacific plate in the late Mesozoic.

© 2011 International Association for Gondwana Research. Published by Elsevier B.V. All rights reserved.

1. Introduction

Recycling of crustal materials at convergent margins has been a key issue in understanding the evolution of lithosphere (e.g., Stern, 2011). Subduction is a major process for the recycling of oceanic crust, through the incorporation of fluids released from the oceanic crust or the melting of itself. However, the identification of subduction-related magmatism in specific regions has been debated, since crustal delamination and contamination are both able to introduce crustal materials into the magma and usually predestine similar whole-rock elemental and isotopic features typical of arc volcanic rocks (e.g., LILE enrichment, Nb and Ta depletion). In spite of the difficulty in determining the role of crustal materials in the arc-like rocks with whole-rock geochemistry, the detailed behaviors of different elements (including LILE) during subduction, identified in recent studies (e.g., Busigney et al., 2003; Spandler et al., 2003; Straub and Layne, 2003a; Rapp et al., 2008), has revealed new fingerprints of arc magmas and the materials that are modified by early-stage subduction which enter into the deeper mantle. Especially, the decoupling of volatiles and LILEs observed by Straub and Layne (2003a), might provide new clues for the determination of subduction process. Moreover, the detrital sediments may also be involved in subduction along with the oceanic slab (Stern, 2011), which might lead to the "zircon effect" (Patchett et al., 1984). This, undoubtedly, will also help uncover potential evidences for subduction in a certain area.

There are a great volume of Mesozoic volcanic rocks in eastern China, and their relationships with the westward and northwestward subduction of Paleo-Pacific plate have been in debate for a long time (e.g., Li, 2000; Li and Li, 2007; Yuan, 2007; Zhang et al., 2008). It has been proposed that the lithosphere of the North China Craton (NCC) was thinned and the thinning accompanied by decratonization took place in the Mesozoic (Fan et al., 2000; Zhang et al., 2002; Yang et al.,

* Corresponding author. Tel.: +86 25 83592185; fax: +86 25 83686016.
E-mail addresses: tangmyes@gmail.com (M. Tang), wxl@nju.edu.cn (X.-L. Wang), xsxu@nju.edu.cn (X.-S. Xu), leo.no1.good@gmail.com (C. Zhu), ctlxy199010212@126.com (T. Cheng), fischer19850910@gmail.com (Y. Yu).
[1] Tel.: +86 25 83686336; fax: +86 25 83686016.

1342-937X/$ – see front matter © 2011 International Association for Gondwana Research. Published by Elsevier B.V. All rights reserved.
doi:10.1016/j.gr.2011.05.009

2010). However, the lithospheric evolution of the South China Block (SCB) seems to be different at the time, since it was not as stable as the NCC, especially during Neoproterozoic time. Determination of the magma source for the Mesozoic volcanic rocks will provide clues for the study of lithospheric recycling and related geodynamic processes. The volcanic rock from the Luzong Basin, which is located in the SCB, adjacent to NCC, is a good target for addressing the puzzling problem. Furthermore, this study will provide insight into the Mesozoic geodynamic framework of eastern China, as the Luzong Basin is a representative one among the five volcanic basins in the lower reaches of the Yangtze River.

Based on the detailed study on apatite geochemistry and zircon U–Pb and Lu–Hf isotopes as well as whole-rock Sm–Nd isotopes from the Luzong volcanic rocks, we recognized a strong Cl–K decoupling in the source and bring out the contrasting Lu–Hf and Sm–Nd isotopic evolution from early to late stages of the volcanic rocks. Integrating with previous geochemical data, the early Neoproterozoic oceanic crust and sediments are proposed to have played an important role in the generation of the volcanic rocks.

2. Geological background

The NCC and SCB are separated by the Qinling orogenic belt in the west and Dabie-Sulu ultra high pressure (UHP) orogenic belt in the east, with the north-striking Tancheng-Lujiang (Tan-Lu) fault cutting through. The SCB is composed of two small blocks integrated by the Jiangnan orogen: the Yangtze Block to the northwest and the Cathaysia Block to the southeast, and both blocks are characterized by distinct geochemical and geochronological record (e.g., Wong et al., 2011; Yao et al., 2011). The Luzong Basin occurs in the southwest Anhui Province, China, located in the northeastern Yangtze Block (Fig. 1). It is bounded by the Tan-Lu fault and the Dabie Orogen to the west and other secondary faults around (Fig. 1). The Luzong volcanic rocks, which are exposed in the Luzong Basin, could be subdivided into four formations: from bottom to top, the Longmenyuan Formation (*F-1*), the Zhuanqiao Formation (*F-2*), the Shuangmiao Formation (*F-3*) and the Fushan Formation (*F-4*). The rocks are generally rich in potassium, with compositions from trachy-basalt to trachyte. Available laser-ablation (LA)-ICP-MS zircon U–Pb dating shows that the volcanic rocks erupted within the duration from 135 Ma to 127 Ma (Zhou et al., 2008).

Contemporaneous volcanic rocks are widespread along the mid-lower reaches of the Yangtze River. As a typical case of the Cretaceous volcanic rocks in the area, the Luzong volcanic rocks have drawn much attention in the last three decades. Although their petrogenesis remains in debate, it has been widely accepted that these rocks formed in an extensional setting (Liu et al., 2002; Wang et al., 2006; Xie et al., 2007). In recent years, progressively more attention has been paid to the lithospheric thinning events in eastern China in the late Mesozoic (Yang et al., 2010; and other references). Available whole-rock geochemical data for the Luzong volcanic rocks show arc-like geochemical features and enriched mantle like isotopic signatures (Wang et al., 2006). However, the mechanism for the enrichment remains unresolved. Liu et al. (2002) argued that the enrichment resulted from the metasomatism by LILE-rich fluids released from the subducted Paleo-Pacific slab in the Mesozoic. Xie et al. (2007) held that delamination, which involved the lower continental crust, was responsible for the isotopic enrichments. Zhang et al. (2011) showed

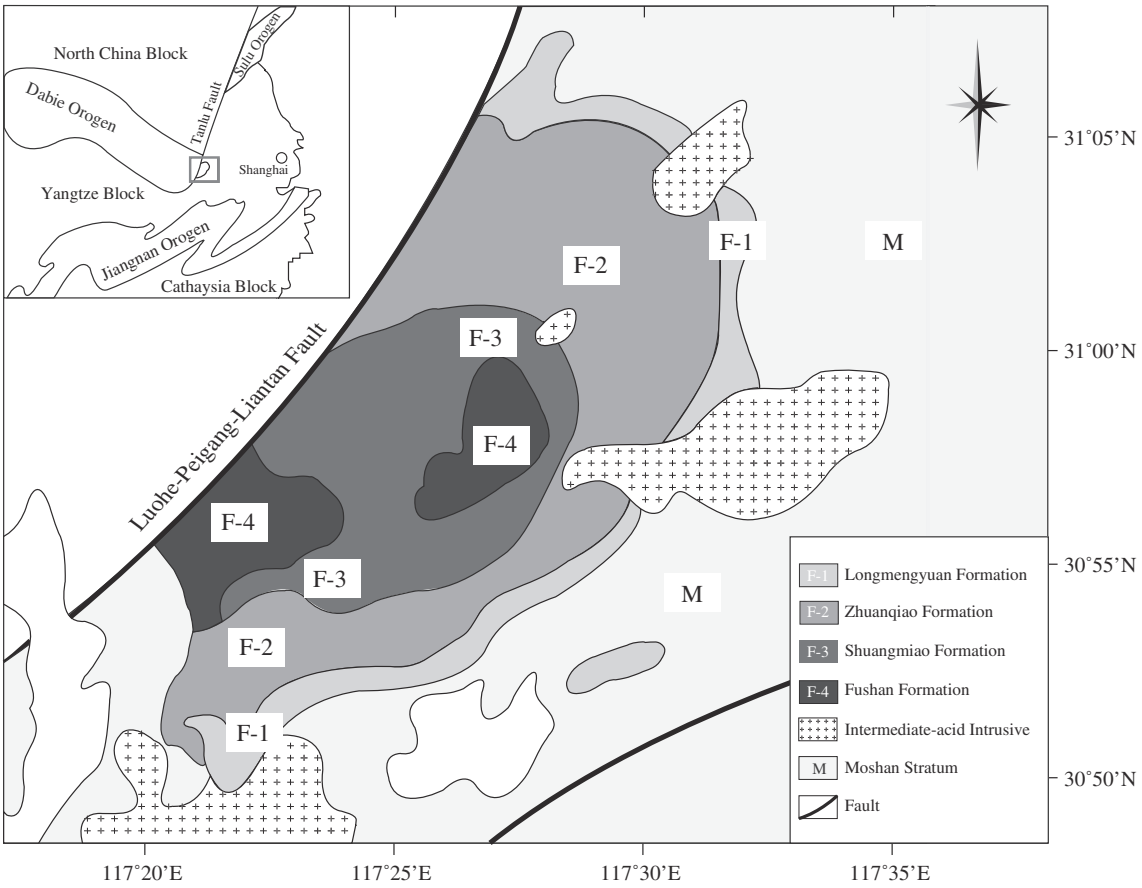

Fig. 1. Geological sketch map of Late Mesozoic Luzong volcanic rocks. The Longmenyuan Formation (*F-1*) is composed of basaltic trachytes and trachy-andesites; the Zhuanqiao Formation (*F-2*) is composed of trachy-andesites and basaltic trachytes; the Shuangmiao Formation (*F-3*) is composed of trachy-basalts and basaltic trachytes; the Fushan Formation (*F-4*) is composed of trachytes and phonolites.

that episodic magmatism in the Paleozoic and Mesozoic modified the composition of the ancient lower crust of the NCC and destroyed the structure of the lithosphere, substantially contributing to the decratonization of the NCC. The incorporation of subducted sediments in the mantle source has also been proposed as a possible mechanism (Wang et al., 2006), but the evidence is inadequate and the timing of the subduction event is unclear. Presently, Paleo-Pacific plate subduction is a model favored by those who viewed the late Mesozoic igneous activities in eastern China from the perspective of subduction-related petrogenesis (e.g., John et al., 1990; Faure and Natal'in, 1992; Lapierre et al., 1997; Li and Zhou, 1999; Li, 2000; Li and Li, 2007; Yang et al., 2011), whereas the Paleo-Pacific plate subduction model does not answer some of the key issues (e.g., most late Mesozoic igneous rocks in eastern China are located too far away from the subducting trench; Shao et al., 2000; Zhang et al., 2001; Yuan, 2007; Zhang et al., 2008).

3. Whole-rock and apatite samples

3.1. The Luzong volcanic rocks

Seven representative samples were collected from the Luzong Basin, including two trachy-andesites from *F-2* (LZ-1, LZ-2), two trachy-basalts from *F-3* (LZ-3, LZ-4), and three trachytes from *F-4* (LZ-5, LZ-6 and LZ-7). The trachy-andesites and trachy-basalts show porphyritic textures, and are mainly composed of plagioclase (60%, An = 28%), clinopyroxene (18%), alkaline feldspar (15%), minor olivine (4%) and accessory biotite, magnetite and apatite. Clinopyroxene and most plagioclase occur as phenocrysts while alkaline feldspar and plagioclase microlite are the dominant components of the matrix. Trachytes generally show trachytic texture, and are mainly composed of alkaline feldspar (70%), plagioclase (10%, An = 10%), minor clinopyroxene (7%) and biotite (5%), accessory magnetite (3%) and apatite. Alkaline feldspar (sanidine) and biotite exist as phenocrysts while matrix mainly consists of alkaline feldspar. The sampling was conducted on fresh outcrops. However, careful microscope observations indicate post-magmatic alteration to different extent, with olivine and clinopyroxene being partly replaced by chlorite and calcite.

3.2. Apatite

Apatite is a ubiquitous accessory mineral, which exhibits euhedral crystal with grain size ranging from 50 μm to 500 μm in length and 30 μm to 100 μm in width. The apatite occurs either as single crystal in groundmass or as inclusions in plagioclase, clinopyroxene, magnetite and in other apatites in all samples from *F-2* and *F-3* (Fig. 2a–c). Apatites are much less common in the samples from *F-4* due to the relatively low whole-rock P contents. The mineral also occurs in groundmass or as inclusions in plagioclase, biotite and magnetite (Fig. 2d). These observations imply that apatites from *F-2* and *F-3* crystallized earlier than plagioclase and clinopyroxene whereas those from *F-4* formed earlier than plagioclase and biotites. BSE images reveal the broad homogeneity of these apatites. Although one of the CL images (Fig. 2e) exhibits weak zoning, later EMPA and laser-ablation ICP-MS studies show little compositional heterogeneity.

4. Analytical methods

Major elements in apatite were determined using a JEOL JXA-8100 electron microprobe at State Key Laboratory for Mineral Deposits Research (MiDeR), Nanjing University (NJU). All analyses were performed under an accelerating voltage of 15 kV, with a beam current of 20 nA and a beam diameter of 1 μm. Standards used in this work include natural apatite for F, Cl, Ca and P, galena for S, hornblende for Na, Si, Mg, and Fe. OH was calculated by site difference (Cl + F + OH = 1 pfu). Each apatite grain was analyzed with 2–10 spots, from core to rim.

All whole-rock samples were prepared by crushing in an agate shatterbox. Major elements and most trace elements were analyzed at ALS Chemex Company (Guangzhou, China), using an X-ray fluorescence spectrometer (XRF) and an ICP-MS, respectively. The analytical precisions for major elements are less than 1%, and 5–10% for most of the trace elements.

Zircon grains were separated from sample LZ-1(*F-2*), LZ-5 and LZ-6 (*F-4*) for U–Pb dating and Lu–Hf isotopic analyses. Trace elements in apatite and zircon U–Th–Pb isotopes were determined using an Agilent 7500a ICP-MS coupled with a New Wave UP213 laser-ablation system at MiDeR, NJU. He carrier gas was used to transport the ablated sample from the standard laser-ablation cell, and then mixed with the Ar gas via a mixing chamber before entering into the ICP-MS torch. All of the spot analyses were carried out using a repetition rate of 5 Hz. The laser-ablation beams are 18 μm and 25 μm in diameter for zircon U–Th–Pb isotopes and apatite trace elements, respectively. NIST610 glass was used as external standard for trace elements with Ca contents (from EMPA) being internal standard. KL-2 glass was used as the reference material to monitor the analytical accuracy. GJ-1 was used for external standard with a recommended $^{207}Pb/^{207}U$ age of 608.5 ± 1.5 Ma (Jackson et al., 2004). Zircon standard Mud Tank (intercept age of 732 ± 5 Ma; Black and Gulson, 1978) was used to monitor the analytical accuracy. U–Pb ages were calculated from the raw signal data using the online software package GLITTER (ver. 4.4) (www.mq.edu.au/GEMOC). The common Pb correction was carried out by using the EXCEL program of ComPbCorr# 151 (Andersen, 2002). The calculations of weighted average ages and plotting on Concordia were finished using the ISOPLOT program (ver. 2.06) of Ludwig (1999). The results are reported in 1σ error.

Dated zircon grains were further analyzed for Lu–Hf isotopes using a Geolas193 laser-ablation system attached to a Nu Plasma HR multi–collector ICP-MS at the State Key Laboratory of Continental Dynamics, Northwest University, Xi'an. Instrumental conditions and data acquisition in detail are described in Yuan et al. (2008). Typical ablation time was about 30 s for 200 cycles, with a 5 Hz repetition rate and a beam diameter of 44 μm (predominantly). He was used as the carrier gas, then combined with argon in a small mixing chamber prior to transport into the ICP torch. In case of the influence of isotopic zoning or with intersecting cracks/inclusions, only the flattest, most stable portions of the time-resolved signal were selected for integration. Isobaric interference of ^{176}Lu on ^{176}Hf was corrected by measuring the intensity of the interference-free ^{175}Lu isotope and using a recommended $^{176}Lu/^{175}Lu$ ratio of 0.02655 (Machado and Simonetti, 2001) to calculate $^{176}Lu/^{177}Hf$ ratios. Correction for isobaric interference of ^{176}Yb on ^{176}Hf was performed in 'real time' as advocated by Woodhead et al. (2004) and developed by Iizuka and Hirata (2005). This involves measuring the interference-free ^{172}Yb and ^{173}Yb during the analysis, calculating mean β_{Yb} value from ^{172}Yb and ^{173}Yb and using a recommended $^{176}Yb/^{172}Yb$ ratio of 0.5886 (Chu et al., 2002) and mean β_{Yb} value to calculate $^{176}Yb/^{177}Hf$ ratios (Wu et al., 2006). Zircon 91500 was used as the reference standard afterwards, with a recommended $^{176}Hf/^{177}Hf$ ratio of 0.282306 ± 10 (Woodhead et al., 2004). The analytical error for single Lu–Hf isotope analysis results is in 1σ. We have adopted a decay constant for ^{176}Lu of 1.865×10^{-11} year^{-1} (Scherer et al., 2001). Initial $^{176}Hf/^{177}Hf$ ratios $\varepsilon_{Hf}(t)$ were calculated with reference to the chondritic reservoir (CHUR) of Blichert-Toft and Albarede (1997) at the time of zircon growth from the magma. Two-stage Hf model age (T_{DM2}) is calculated relative to the depleted mantle with present-day $^{176}Hf/^{177}Hf$ = 0.28325 and $^{176}Lu/^{177}Hf$ = 0.0384 (Nowell et al., 1998; Griffin et al., 2000), bulk crust with present-day $^{176}Lu/^{177}Hf$ = 0.015 (Griffin et al., 2002).

The Nd isotopic compositions were determined using the ID-TIMS (Finnigan MAT Triton TI) at MiDeR, NJU. Chemical separation procedures

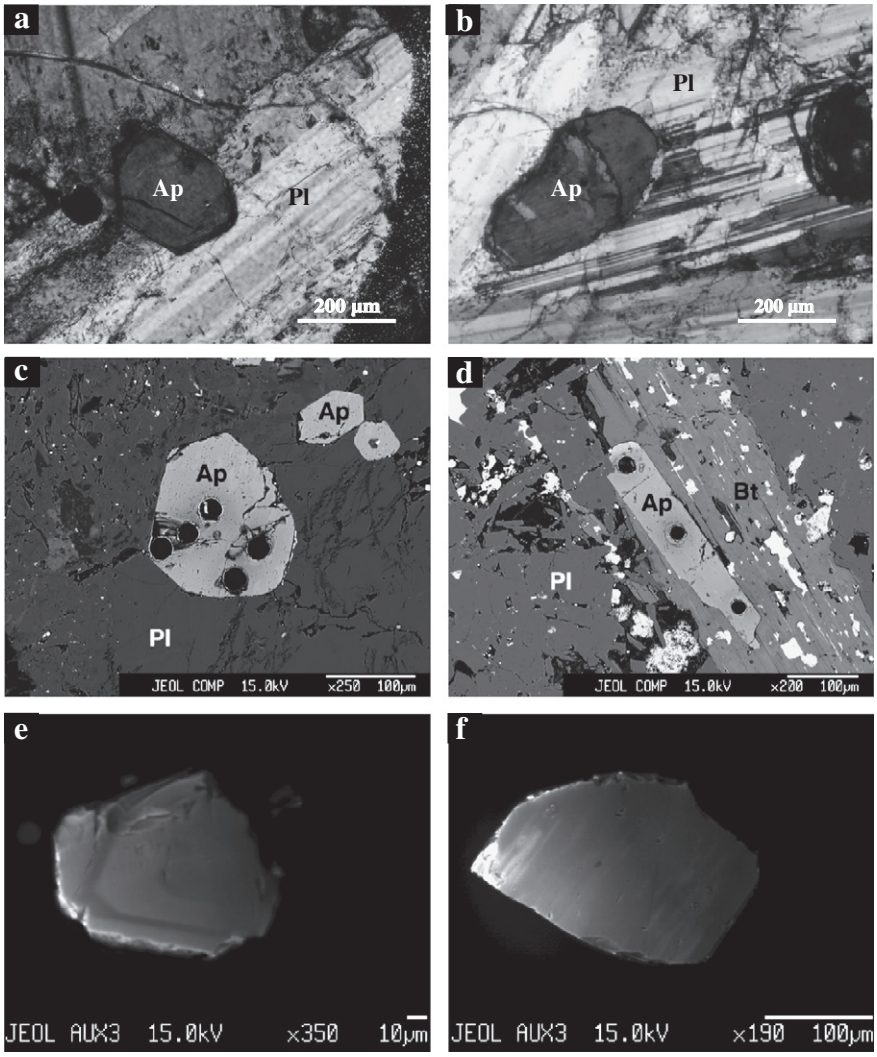

Fig. 2. (a) and (b): Photomicrographs of apatites from the Luzong volcanic rocks (crossed nicols); (c) and (d): Back scattered electron images; (e) and (f): Cathodoluminescence (CL) images. Note that apatites are quite homogeneous in BSE images and slightly exhibit zonation in CL images. Ap = apatite, Pl = plagioclase, Bt = biotite.

follow Pu et al. (2005), with relative standard deviation (RSD) lower than 5×10^{-6}. Mass fractionation was corrected according to $^{146}Nd/^{144}Nd = 0.7219$. The long-term $^{143}Nd/^{144}Nd$ analyzing value of the international standard JNdi-1 is 0.512121 ± 0.000016 (2σ, n = 67), consistent with the value (0.512115 ± 0.000007) of Tanaka et al. (2000). The $\varepsilon_{Nd}(t)$ values were calculated based on the Nd isotopic compositions of $^{143}Nd/^{144}Nd$ (CHUR) = 0.512638 and $^{147}Sm/^{144}Nd$ (CHUR) = 0.1967.

5. Results

5.1. Whole-rock major and trace elements

A TAS classification was applied for our samples, as shown in Fig. 3. Samples from all three formations display enrichments of LILEs (K, Rb, Sr, Ba, Pb, U, etc.), which is typical of arc volcanic rocks (Fig. 4). The LREEs are enriched relative to HREEs, while the HFSEs (Nb, Ta, Ti) are obviously depleted. However, it should be noted that the abundances of incompatible elements of the Luzong volcanic rocks are significantly higher than those of typical arc volcanic rocks but close to that of global subducting sediment (GLOSS) calculated by Plank and Langmuir (1998). Detailed data are available in Background Dataset 1.

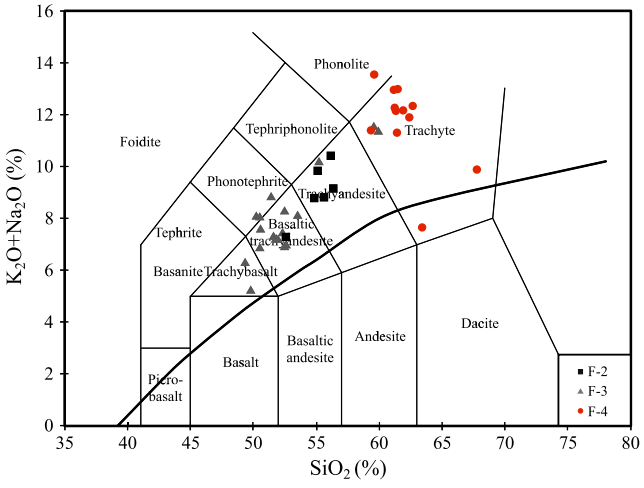

Fig. 3. TAS diagram for the Luzong volcanic rocks. Data from Liu et al. (2002), Wang et al. (2006), Xie et al. (2007) and this study.

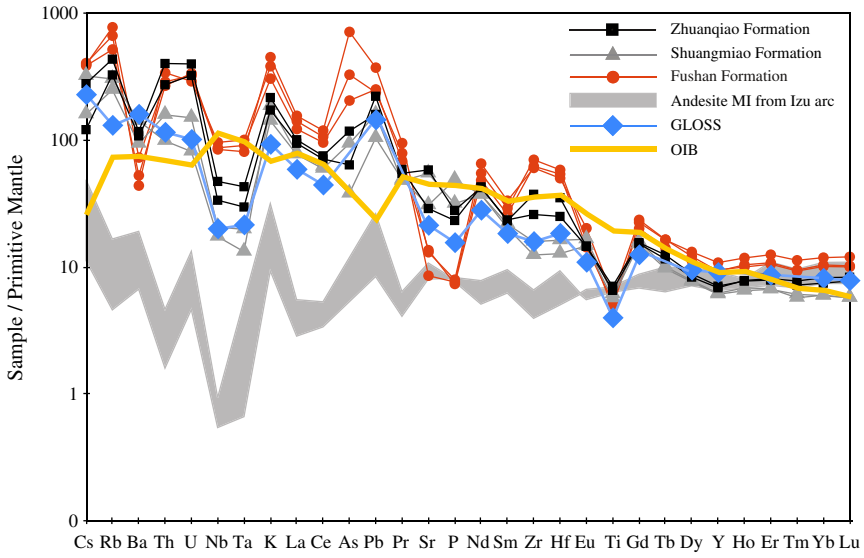

Fig. 4. Primitive mantle normalized spider diagram for the Luzong volcanic rocks, in comparison with GLOSS and arc andesite MI. GLOSS is from Plank and Langmuir (1998); arc andesite MI compositions are from Straub and Layne (2003a); OIB composition is from Sun and McDonough (1989). Primitive mantle composition is from Lyubetskaya and Korenaga (2007).

5.2. Apatite composition

5.2.1. Major elements

Apatites from the Luzong volcanic rocks are generally fluorapatites, while these apatites are also high in hydroxyl, especially for samples from *F-4*. Detailed data are available in Background Dataset 2. It should be noted that nearly all these apatites contain extremely low chlorine (<1000 ppm). Na_2O is hardly detected in apatites from *F-2* and *F-3*, while apatites from *F-4* have relatively higher Na_2O (1000–2000 ppm) and SiO_2 (500–1000 ppm). Additionally, apatites from *F-4* have relatively low MgO and FeO, indicating the melt in equilibrium with the apatites is more evolved.

5.2.2. Trace elements

As a mineral phase that crystallizes at early stage, apatite could be used to probe into the melt composition in the magma chamber. Profile composition indicates that most major and trace elements exhibit neglectable variation from core to rim, which agrees well with previous BSE observations. Detailed data are available in Background Dataset 3. Generally, apatites from the three formations of the Luzong Basin have similar REE patterns (Fig. 5). Eu(II) and Eu(III) have different partitioning coefficients between apatite and melt due to their different ion radii (Watson and Green, 1981). Therefore, δEu in apatite is co-controlled by the δEu and the Eu(II)/Eu(III) ratio in the melt when apatite crystallizes. Whole-rock δEu changes insignificantly from LZ–1 to LZ-7. In addition, most apatite grains occur as inclusions in plagioclases, suggesting their earlier crystallization. Therefore, the constant δEu values (most analysis ranging from 0.40 to 0.50) in all analyzed grains require that the Eu(II)/Eu(III) ratio in the melts in equilibrium with the apatites vary little from LZ1 to LZ-7. The $\sum$REE contents in apatites from *F-4* are remarkably higher than those in apatites from *F-2* and *F-3*, consistent with the relatively low CaO, MgO and FeO contents in the apatites from *F-4*. This might be caused by relatively late crystallization of apatites from *F-4* because REE partition coefficients between apatite and melt increase with increasing degree of polymerization of the melt (Prowatke and Klemme, 2006).

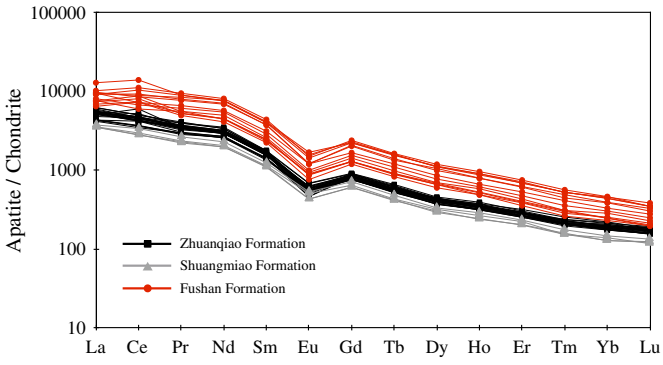

Fig. 5. Chondrite-normalized REE pattern diagram for apatites from the Luzong volcanic rocks. Chondrite value is from Sun and McDonough (1989).

Other trace elements provide further information about the source and magma evolution. Firstly, Sr drops dramatically in apatites from *F-4*, consistent with the observation in whole-rock composition. The loss of Sr has often been interpreted as a result of fractional crystallization of plagioclase due to the large partitioning coefficient of Sr in plagioclase (Drake and Weill, 1975). However, it is not the case for the volcanic samples from *F-4*. The apatite grain LZ-6-06 from *F-4* is included in plagioclase, suggesting that its formation might have not been affected by the fractional crystallization of plagioclase, but this grain still has fairly low Sr content (382–406 ppm) compared with apatites (Sr>1000 ppm) from *F-2* and *F-3*. Therefore, low Sr contents in apatites and whole rocks of *F-4* should be a feature inherited from the magma source, rather than the results of fractional crystallization. Secondly, Zr, U and Th contents increase systematically from *F-2* and *F-3* to *F-4* in whole rocks while such increase is neglectable in apatites. A possible explanation may refer to the crystallization of zircon which is the major reservoir of Zr, U and Th. The low Zr, U and Th contents of apatites from *F-4* suggest that zircons might crystallize earlier than apatites in the case of *F-4*. This is also supported by its highest zircon saturation temperature among the three formations (Wang et al., 2006).

5.3. Zircon dating and Lu–Hf isotopes

Zircons from all samples are clear and transparent, typically 50–150 μm long and 30–100 μm wide. All zircon grains display prismatic and pyramidal crystal faces, among which, most grains exhibit weakly oscillatory zonation (Fig. 6). Contents of Th (89–5106 ppm) and

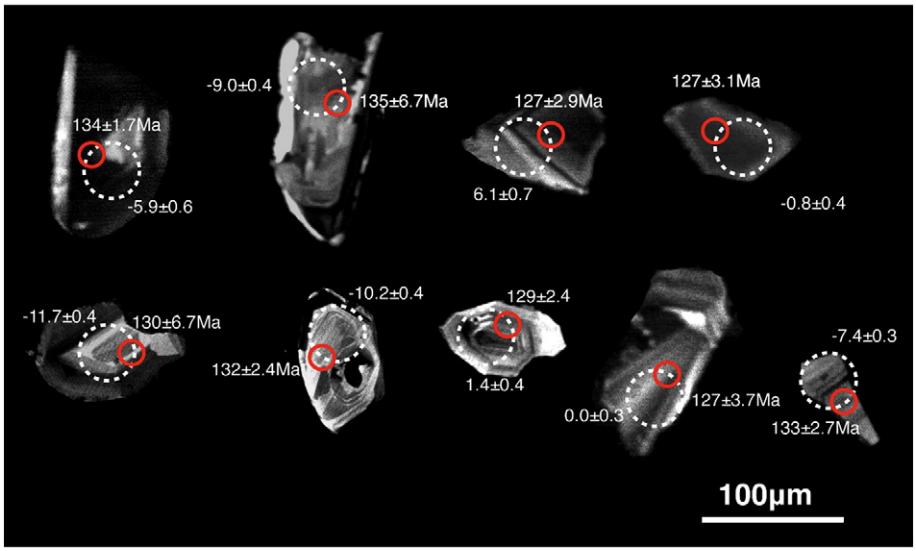

Fig. 6. Cathodoluminescence (CL) images of representative zircons from the Luzong volcanic rocks. Small red circles are spots for U–Pb isotopes using LA–ICPMS, and big white dashed circles are spots for Hf isotopes using LA-MC-ICPMS.

U (34–1815 ppm) are high and varying with Th/U ratios ranging from 0.42 to 20.89. Detailed data for zircon U–Pb dating are available in Background Dataset 4.

All of the zircons separated from LZ-1 are concordant in Fig. 7a. The analyzed zircons yield a weighted mean $^{206}Pb/^{238}U$ age of 132 ± 1.5 Ma (MSWD = 0.37, n = 14) for *F-2*. 25 of the zircon grains separated from LZ-5 and LZ-6 are concordant and these ages were adopted when calculating the ages (Fig. 7b). The main population of zircons yield a weighted mean $^{206}Pb/^{238}U$ age of 129 ± 1.2 Ma (MSWD = 1.03, n = 25) for *F-4*.

Zircons from *F-2* and *F-4* have been further studied for *in situ* Hf isotopes and the detailed data are available in Background Dataset 5. Zircons $\varepsilon_{Hf}(t)$ values of *F-2* show a small variation and yield a mean value of −10.3. However, the values of zircons from *F-4* (LZ−5 and LZ-6) have relatively large variations (from −7.9 to +6.1), which might result from the incorporation of zircons from earlier erupted rocks (e.g. *F-2*, *F-3*) during magma upwelling. Apart from three zircons from *F-4* with rather low $\varepsilon_{Hf}(t)$ (< −5), the other grains have $\varepsilon_{Hf}(t)$ values ranging from −2.6 to +6.1, constituting a normal distribution. We thus eliminated the low-$\varepsilon_{Hf}(t)$ zircon grains (LZ-5-06, LZ-5-08 and LZ-5-11) when calculating mean $\varepsilon_{Hf}(t)$ for *F-4*. Contrasting differences in both $\varepsilon_{Hf}(t)$ values and zircon two-stage Hf model ages exist between *F-2* and *F-4* (Fig. 8). $\varepsilon_{Hf}(t)$ rises notably from *F-2* (mean = −10.3) to *F-4* (mean = +1.2). Zircon two-stage Hf model age peak of *F-2* occurs at around 1.8 Ga while *F-4* around 1.2 Ga.

Nd isotopic data of the Luzong volcanic rocks are listed in Background Dataset 6. Basaltic trachytes (LZ-1 and LZ-2) from *F-2* have $\varepsilon_{Nd}(t)$ ranging from −3.89 to −4.28, similar to that of trachytes (LZ-5, LZ-6 and LZ-7) from *F-4* (−3.03 to −4.17). Trachy-basalt (LZ-3) from *F-3* has a lower $\varepsilon_{Nd}(t)$ (−7.99). Two-stage model ages for Nd vary insignificantly from *F-2* to *F-4* (1.3-1.2 Ga), except that LZ-3 has a relatively old age (ca. 1.6 Ga).

6. Discussion

Apatite can be a secondary mineral and crystallize at post-magmatic alteration stage. However, it is not the case for the apatites from the Luzong volcanic rocks because most apatite grains analyzed occur as inclusions in plagioclase, and those grains in groundmass display little compositional differences compared with those occurring as inclusions. The zircon grains are also believed to be primary

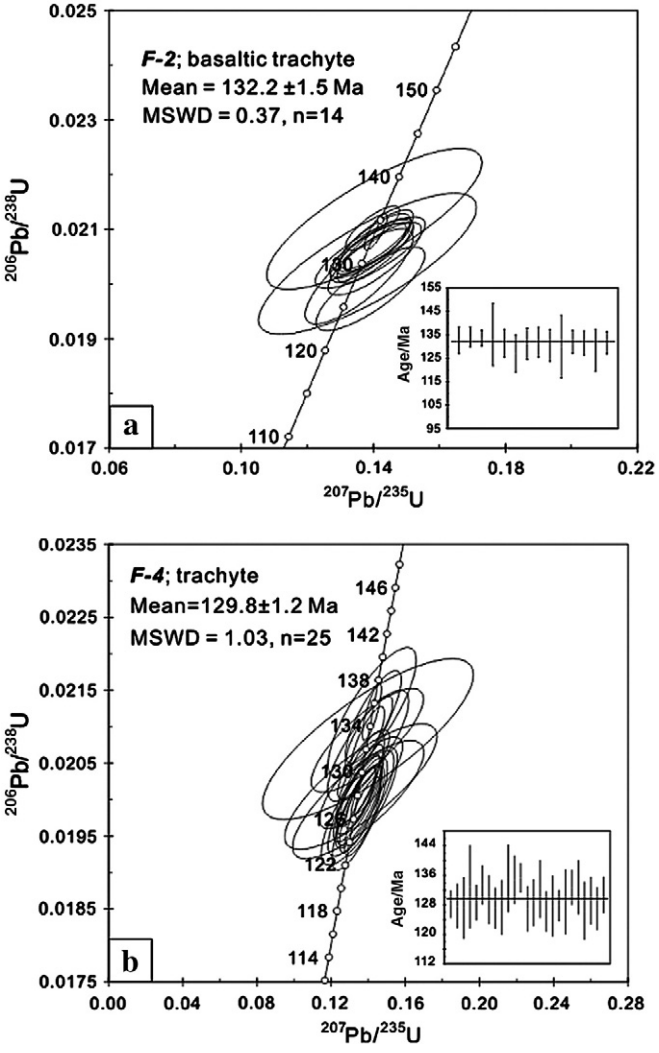

Fig. 7. Zircon U–Pb concordia diagram for volcanic rocks from the Zhuanqiao (a) and Fushan Formation (b).

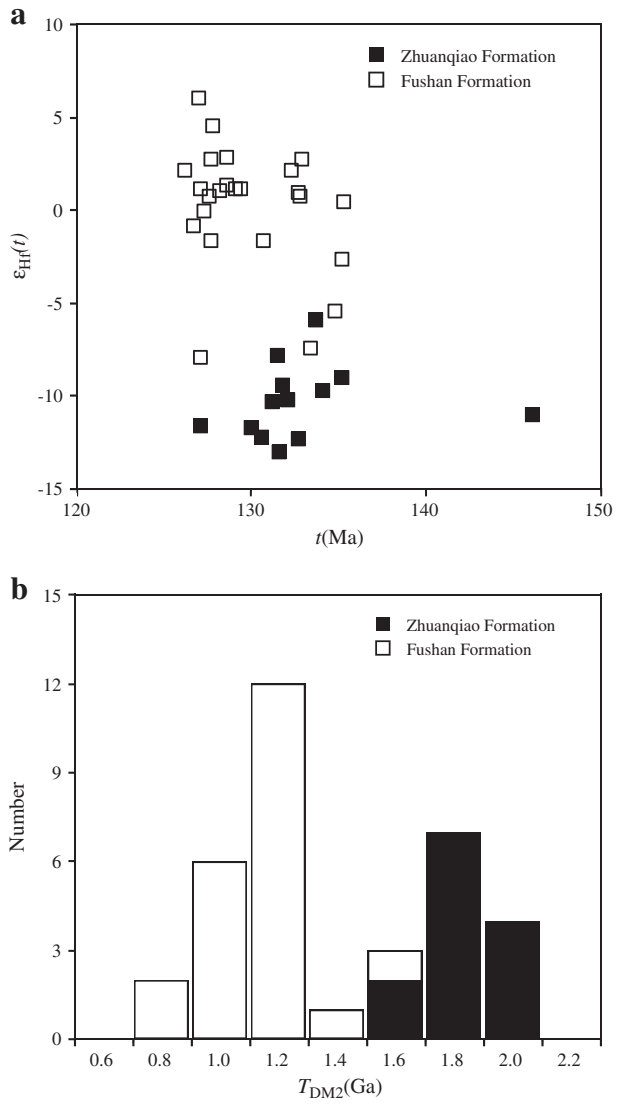

Fig. 8. Plot of zircon $\varepsilon_{Hf}(t)$ vs. ages (a) and histogram of zircon two-stage Hf modal ages (T_{DM2}) (b) for the Zhuanqiao and Fushan Formation samples (LZ-1, LZ-5 and LZ-6).

magmatic because of their euhedral form, weak oscillatory zonation, high Th/U ratios, and their U–Pb ages which are consistent with the previous dating results (Zhou et al., 2008, and the references therein concerning K-Ar and Rb–Sr dating).

Before we address the petrogenesis of the volcanic rocks, the role of crustal contamination should be evaluated, because large-scale crustal contamination can produce a melt similar to what stems from an enriched mantle or arc volcanic rocks (e.g., Dungan et al., 1986; Wolff et al., 2005). Based on the available geochemical data, crustal contamination may be insignificant for the generation of the Luzong volcanic rocks. Firstly, Sr–Nd isotopic studies from previous authors (e.g., Liu et al., 2002; Wang et al., 2006 and Xie et al., 2007) found no co-variation in $\varepsilon_{Nd}(t)$ *vs.* SiO_2 and $(^{87}Sr/^{86}Sr)_i$ ratios *vs.* 1/Sr. Secondly, the negative correlation between La/Nb ratios and SiO_2 contents in whole rock (Fig. 9) also precludes significant crustal contamination.

6.1. Low Cl/K ratio in the Luzong volcanic rocks

6.1.1. Extremely low Cl apatites

According to the available geochemical data, most apatites from intermediate igneous rocks, especially andesites originated from subduction-related settings, have relatively high chlorine contents

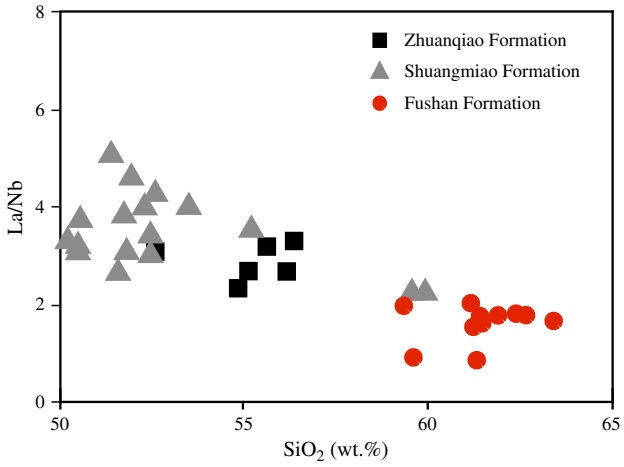

Fig. 9. Plot of La/Nb vs. SiO_2. Data from Liu et al. (2002), Wang et al. (2006), Xie et al. (2007) and this study.

(Boyce and Hervig, 2009), while the apatites from granites, especially S-type granites, contain much less chlorine (Sha and Chappell, 1999). The overall high F and low Cl contents in apatites from S-type granites are interpreted to mainly reflect the halogen abundances in the sedimentary source rocks, since they had experienced a relative enrichment of F and preferential loss of Cl during prior weathering process, because of the high solubility of Cl in aqueous solutions (Brehler and Fuge, 1974). Apatites from the Luzong volcanic rocks are characterized by low Cl contents, even lower than apatites from S-type granites (Fig. 10).

Halogen degassing might result in low-Cl contents in apatites. But halogen degassing takes place only when magma gets very near the surface (e.g., <200 MPa; Aiuppa et al., 2004; Stelling et al., 2008). As for the Luzong apatites, neither major nor trace element compositions exhibit remarkable variations from core to rim in these large-size grains (50–500 μm). Such compositional homogeneity requires stable crystallizing conditions for the apatites, including melt composition, temperature and pressure. Moreover, our apatites, as estimated above, crystallized earlier than plagioclase and even clinopyroxene.

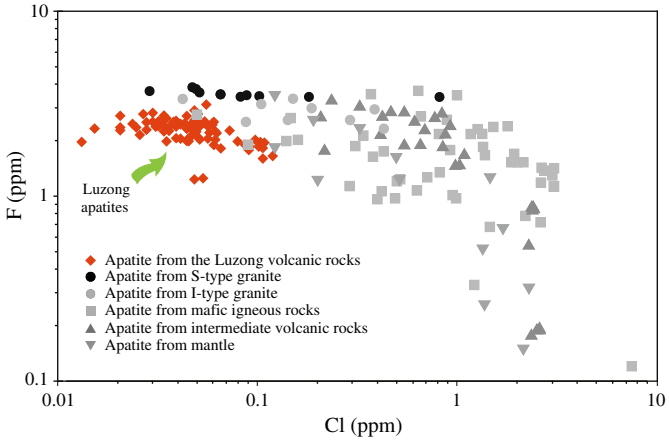

Fig. 10. Logarithmic plot of halogen composition of apatites from the Luzong volcanic rocks, in comparison with apatites from different types of igneous rocks. Data sources, apatites from mafic igneous rocks: Brearly and Jones (1998), Min et al. (2003), McCoy et al. (1996), Semenenko et al. (2004), Kurat et al. (2002), Folco et al. (2004), Boudreau and McCallum (1989), Huntington (1979), Nash (1976), Willmore et al. (2000), Boudreau et al. (1995), Warner et al. (1998), Fodor (2001), Meurer and Natland (2001), Spengler and Garcia (1988); apatites from I-type and S-type granite: Sha and Chappell (1999); apatites from intermediate volcanic rocks: Peng et al. (1997), Boyce and Hervig (2009); apatites from mantle: O'Reilly and Griffin (2000).

Hence, a deep magma chamber with stable P–T condition may be appropriate for the generation of these apatites, which implies that the occurrence of halogen degassing is unlikely to have occurred.

Brenan (1993) noted that the rapid cooling of eruptive and hypabyssal magmatic systems prevented the diffusion of halogen from the magma, and thus the apatites trapped as inclusions in other minerals might preserve the initial halogen chemistry of magma source (Webster et al., 2009). Piccoli and Candela (2002) pointed out that volcanic apatites rarely exhibit chemical zoning, well consistent with the observation of this work. Thus, it could be concluded that apatites from the Luzong volcanic rocks are free from post-magmatic diffusion of halogens and may preserve the initial information of the halogen composition of the parental melt. Therefore, these low-Cl apatites reflect the low Cl concentration in the parental magma, which is a feature inherited from the source.

Fluorine and chlorine are both incompatible elements, their contents vary with the fractionation of melt. Therefore parameters that index fluorine and chlorine to other highly incompatible elements have been introduced to study halogen compositions of the source. K is commonly used (e.g., Aoki et al., 1981; Jambon et al., 1995; Douce and Roden, 2006) because F/K and Cl/K ratios vary within narrow ranges among continental basalts, MORB and OIB samples that are not contaminated by seawater. Arc volcanic rocks exhibit significantly elevated Cl/K ratios due to the large incorporation of Cl released from the altered oceanic crust and sediments during early-stage subduction. In fact, in addition to F/K and Cl/K ratios, other ratios (e.g., F/P, Cl/Nb and etc.) were also frequently adopted, since these element pairs are similarly incompatible (Schilling et al., 1980).

The Luzong volcanic rocks are rather enriched in K, strongly contrasting with the extremely low Cl contents in apatites. In fact, the Luzong volcanic rocks generally have much higher K contents than those referred in Fig. 10 while the Luzong apatites have the lowest Cl contents. It is unrealistic to expect a sort of melt with normal Cl/K ratio to produce such low-Cl apatites and high-K whole rocks simultaneously, when potential loss of Cl during syn- and post-magmatic processes has been eliminated. An alternative explanation is the Cl–K decoupling in the source.

A low Cl/K ratio source is required to be responsible for the low-Cl apatites and high-K contents in whole rocks. The incorporation of lower continental crust in the mantle source, as suggested by Xie et al. (2007), is unable to produce a magma with low Cl/K ratio because Cl/K ratio of lower continental crust (~0.05; Rudnick and Gao, 2004) is believed to fall in the variation range of uncontaminated MORB (i.e. 0.01–0.07; Michael and Cornell, 1998). Moreover, crustal delamination would more likely produce Cl–Nb decoupling, instead of Cl–K decoupling, because Nb might be trapped in rutile in the residue (Hermann and Rubatto, 2009). Since Nb is also depleted in the Luzong volcanic rocks, Cl–Nb decoupling may be insignificant. Contamination of middle and/or upper continental crust is able to decrease Cl/K ratio in the magma (Rowe and Lassiter, 2009). However, large crustal contamination is unlikely as discussed above. Moreover, it remains rather questionable whether crustal contamination alone can produce such low–Cl apatites because apatites from S-type granite have even higher Cl contents. Meanwhile, apatites from continental basalts, as far as we are aware of, have much higher Cl contents than the Luzong apatites.

6.1.2. A possible mechanism responsible for the low Cl/K ratio

The low Cl/K ratios of the Luzong volcanic rocks might be accomplished in two steps.

As one of the most soluble elements in aqueous solutions (Brehler and Fuge, 1974), Cl tends to be lost during weathering. In contrast, K and F are much more conservative due to their relatively low migration rate, resulting in the low Cl/K ratios of continental detritus. And this is why Cl is depleted in upper continental crust, because Cl is transported to the oceans and accumulates in seawater (Pyle and Mather, 2009).

When the detrital sediments were transported into subduction trench, the Cl concentration might be elevated to a certain extent through the interaction with seawater which contains as much as 20,000 ppm Cl. But the following dehydration process during the early-state subduction is able to completely remove the Cl buried in the subducted detrital and pelagic sediments (Straub and Layne, 2003b).

Weathering and dehydration are both able to remove Cl in rocks but the latter process, subduction-related dehydration, might be more efficient in Cl-extraction. Much work has been done to quantitatively assess the amount of halogens and LILEs that survive the early-stage subduction and enter into the deeper mantle. Straub and Layne (2003b) estimated that nearly all Cl recycled into the mantle wedge during shallow subduction. Lassiter et al. (2002) argued that Cl retained in deep recycled crust was less than 50 ppm after the extraction during subduction. Scambelluri et al. (2004) calculated that about 45 ppm Cl was hosted in the residual high pressure minerals of subducting oceanic slab. However, F extraction is not as efficient as Cl during early-stage subduction. For example, only 4-5% F was recycled at the Izu arc, leading to the strong fractionation of F from Cl and H_2O (Straub and Layne, 2003b). F contents in sediments vary in a large range, depending on the rock type of sediments. Pelagic clay contains as much as 1300 ppm F (Li and Schoomaker, 2003) while continent-derived sediments might contain about 600 ppm F, similar to the upper crust (Straub and Layne, 2003b). As for LILEs, geochemical studies of meta-sedimentary rocks in the western Alps (Busigney et al., 2003) suggested that LILEs behaved rather conservatively and were not significantly lost during subduction-related devolatilization (Busigney et al., 2003; Spandler et al., 2003). Decoupling between volatiles and LILEs was observed in halogen-rich andesite melt inclusions from the Izu arc volcanic front (Straub and Layne, 2003a). A continuous series of hydrous phases (e.g., amphibole, lawsonite, muscovite, phengite, paragonite, epidote-group minerals, phase egg, K-hollandite) would be stable in subducted continental sediments down to a depth with 15 GPa in pressure (Schmidt, 1996; Ono, 1998; Hermann and Green, 2001; Hermann, 2002; Spandler et al., 2003; Rapp et al., 2008). LILEs released from a decomposed hydrous phase could be re-trapped into another hydrous phase that is stable in higher metamorphic grades. Thus, the whole-rock budget of LILEs in deeply subducted sediments may stay broadly unmodified when passing through the sub-arc regime (Rapp et al., 2008).

There is increasing evidence to suggest that dehydration processes which take place during early subduction are able to fractionate Cl from F and LILEs. Dehydrated residue might be rather low in Cl but still rich in LILEs, as is the key to the Cl–K decoupling in the source.

6.1.3. A four-end-member source model—implication from calculated Cl/K, Cl/Nb and F/K ratios

Since apatites from the Luzong volcanic rocks have rarely undergone obvious subsequent re-equilibration with late-stage fluids or melts, they provide an ideal opportunity to calculate the halogen compositions of the melt. Boyce and Hervig (2009) gave a detailed study on the halogen composition of the volcanic rocks from Irazú volcano formed in 1963 and 1723 eruptions. Samples from the two eruptions have weak whole-rock compositional differences comparing with those from *F-2* and *F-3*. Therefore, we choose their partitioning coefficients for fluorine ($D_F = 15$) and chlorine ($D_{Cl} = 5$) between apatite and silicate melt. As for *F-4*, calculation of halogen compositions for the melt was given up because of the relatively larger compositional variations in whole rock.

The influence of fractional crystallization should be evaluated before using whole-rock K content as that of the melt in equilibrium with apatites. Prowatke and Klemme (2006) observed that REE partitioning coefficients between apatite and melt increase with

increasing degree of polymerization of the melt. Their study outlined the Sm partitioning coefficient array with increasing SiO_2 in the melt. Accordingly, a modeling has been carried out to estimate the extent of fractional crystallization after the crystallization of apatite, by comparing the whole-rock SiO_2 contents with the assessed SiO_2 content in the melt in equilibrium with apatite (Fig. 11). The cross range estimates that SiO_2 in the melt when apatite crystallizes is 54% to 57%, which is slightly higher than the whole-rock SiO_2 contents of samples from *F-2* and *F-3*. This might be caused by the involvement of earlier crystallized, low-SiO_2 phases (e.g., olivine) into the magma after apatites had crystallized. Anyway, fractional crystallization, which might lead to underestimated ratios like Cl/K in our calculation, is insignificant.

There might still be other unknown factors that may affect the accuracy of this calculation. But these do not hamper our discussion of the Cl–K decoupling in the source. As an attempt, this calculation helps quantify the Cl–K decoupling and helps better illustrate source compositions.

The calculated halogen and related element ratios are listed in Table 1. Cl/Nb ratios (3.49–13.88) are roughly between that of N-MORB (~11; compiled from Sun and McDonough, 1989) and primitive mantle (~3; Lyubetskaya and Korenaga, 2007) and F/P values (0.35–1.07) between that of N-MORB (~0.4; compiled from Sun and McDonough, 1989) and crust (~1; Rudnick and Gao, 2004). Obviously, F/K ratios of our samples generally fall on the array defined by MORBs, OIBs, arc volcanic rocks and continental basalts (Fig. 12). As to the Cl/K ratios, the story is totally different. Extremely low Cl/K ratios (<0.004), even lower than in uncontaminated MORBs (i.e. 0.01–0.07; Michael and Cornell, 1998), make the volcanic rocks of *F-2* and *F-3* strongly deviate from the array (Fig. 12), indicating that chlorine decouples with potassium remarkably.

Four possible end-members, including dehydrated altered and unaltered oceanic crust, dehydrated sediments and depleted mantle, are introduced to model the source. Conservative elements, like Nb and Ta, are expected to be free of modification through subduction due to their immobility in fluid. Hence, we refer to GLOSS (Plank and Langmuir, 1998) for LILEs and Nb concentrations of dehydrated sediments.

As summarized in Table 2, sediments and altered oceanic crust that survive the subduction-related dehydration do display extremely low Cl/K ratios, as is associated with the decoupling between volatiles and LILEs at arc front which is marked by high Cl/K ratio. F/K, Cl/Nb and Cl/K ratios of the Luzong volcanic rocks generally plot in the ranges

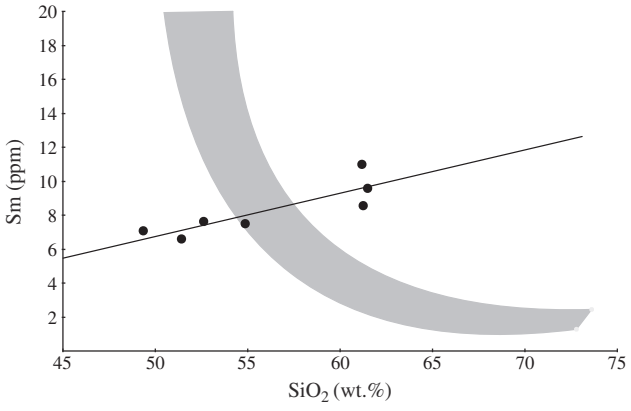

Fig. 11. Plot of Sm vs. SiO_2 concentrations in the melt. Black line represents the evolving trend of Sm concentration in the melt estimated from whole-rock data. Grey belt represents estimated Sm concentration in the melt which is in equilibrium with apatites from the Luzong volcanic rocks (see Prowatke and Klemme (2006) for detailed relationship between Sm partitioning coefficient and SiO_2 in the melt). The cross range of the black line and the grey belt corresponds to the estimated variation range of SiO_2 content in the melt during the apatite crystallization.

Table 1
Calculated halogen concentrations (ppm) in the melt.

	LZ-1	LZ-2	LZ-3	LZ-4
F[a]	1640 (136)	1547 (183)	1518 (142)	1108 (341)
Cl[a]	76 (22)	85 (28)	84 (24)	111 (48)
K[b]	41,300	32,900	27,100	35,400
Nb[b]	21.8	15.5	9.5	8.0
P[b]	1530	1820	2070	3190
Cl/K	1.84×10^{-3}	2.58×10^{-3}	3.10×10^{-3}	3.14×10^{-3}
Cl/Nb	3.49	5.48	8.84	13.88
F/P	1.07	0.85	0.73	0.35
F/K	0.040	0.047	0.056	0.031

1σ of calculated melt F and Cl contents reported in terms of last significant digits in the parentheses.
[a] Based on $F\ (Cl)_{melt} = F\ (Cl)_{\text{average of EMPA data}} / D_{F\ (Cl)}$.
[b] Comes from whole-rock data.

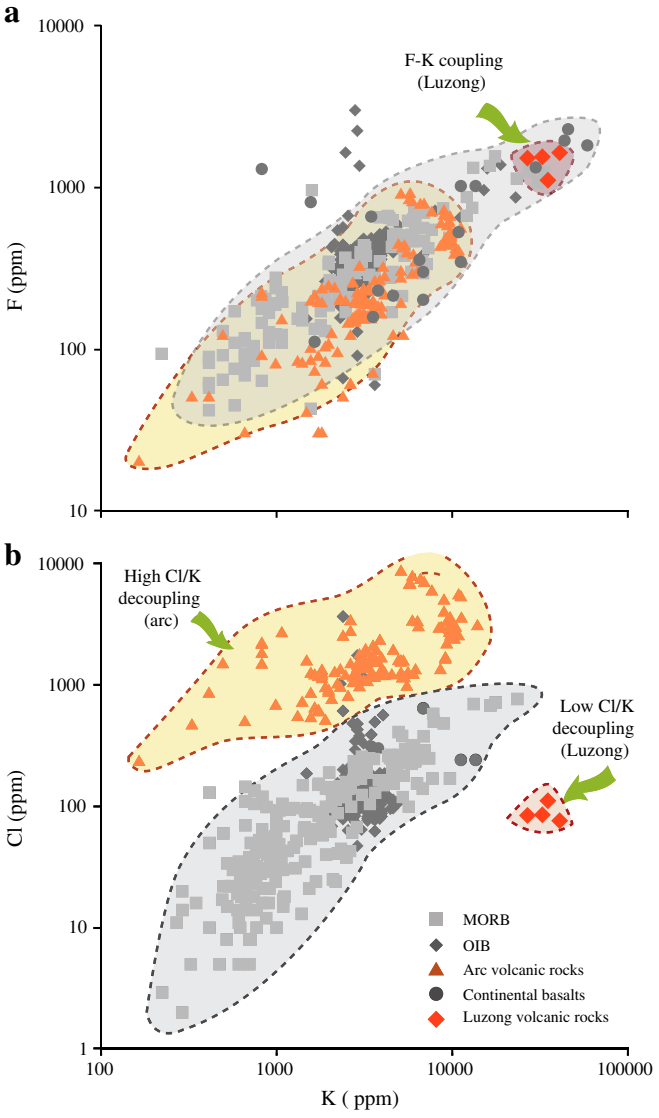

Fig. 12. Plots of halogens vs. K, comparing the Luzong volcanic rocks with MORB, OIB, arc volcanic rocks and continental basalts. F generally develops a good coupling with K in different igneous rocks including the Luzong volcanic rocks. In the case of Cl/K ratio, both arc and the Luzong volcanic rocks deviate from the Cl–K coupling array but stretch to opposite sides. Data sources, MORB: Sigvaldason and Óskarsson (1986); Michael and Cornell (1998); Moune et al. (2007); PETBD database: http://beta.www.petdb.org/. OIB: Aoki et al. (1981); Hansteen and Gurenko (1998); Davis et al. (2003). Arc volcanic rocks: Straub and Layne (2003a). Continental basalts: Aoki et al. (1981); McHone (2002).

Table 2
Summary of Cl, F, K and Nb concentrations in the four possible end-members in the source.

	Luzong volcanic rocks	Dehydrated unaltered oceanic crust[a]	Dehydrated altered oceanic crust[b]	Dehydrated sediments[c]	Depleted mantle[d]
F ppm	1108–1640	100	/	611–1300	11
Cl ppm	76–111	45	45	45	0.51
K ppm	$(2.71–4.13)\times10^4$	1250	2.68×10^4	1.69×10^4	60
Nb ppm	8.0–21.8	2.20	3.56	8.94	0.21
F/K	0.03–0.06	0.08	/	0.04–0.08	0.183
Cl/K	$(1.84–3.14)\times10^{-3}$	36×10^{-3}	1.68×10^{-3}	2.65×10^{-3}	8.50×10^{-3}
Cl/Nb	3.49–13.88	20.45	12.64	5.03	2.43

45 ppm is estimated as an average Cl concentration of dehydrated altered/unaltered crust plus sediments as a whole.
Slash represents data not available.
Note that GLOSS represents an average composition of subducted sediments. More continent-derived sediments involved in the source might still lower the Cl/K ratio of dehydrated sediments. Moreover, we use the original abundance of F in sediments as that of dehydrated sediments so that the F/K ratio of completely dehydrated sediments estimated here should be regarded as an upper limit.
[a] Compiled from Taylor and McLennan (1985) and Michael and Cornell (1998).
[b] K and Nb concentrations estimated according to ODP Sites 801 and 1149 (Kelley et al., 2003).
[c] See text for data sources.
[d] Depleted mantle composition according to Salters and Stracke (2004).

defined by dehydrated altered and unaltered oceanic crust, dehydrated sediments and depleted mantle. Therefore, it is possible that the halogen compositions of *F-2* and *F-3* were produced by mixing some or all of the four end-members, but at least one of the two low-Cl/K end-members (dehydrated sediments and dehydrated altered crust) is required to be present in the source. Because K abundances of dehydrated sediments and dehydrated altered oceanic crust are higher than unaltered crust and depleted mantle by more than a magnitude, even a small input of the low-Cl/K end-members would strongly affect the Cl/K ratio in the source. For example, an ideal source model consisting of 70% from depleted mantle, 10% from dehydrated sediments and 10% from dehydrated altered oceanic crust as well as 10% from dehydrated unaltered oceanic crust (all in wt.%) renders a Cl/K ratio as low as 0.003, close to a source model composed of pure dehydrated sediments or dehydrated altered oceanic crust. So the mixing proportion of the four end-members might not be significant as long as either of the two low-Cl/K end-members is present in the source. Cl/Nb and F/K ratios of the four end-members outline relatively narrow variation ranges. Mixture of them in any proportion would produce the final Cl/Nb and F/K ratios similar to those of *F-2* and *F-3*.

We did not calculate the halogen contents in the melt of *F-4*, but the similar low-Cl apatites and the even higher K contents in whole rocks seem to promise the similar low Cl/K ratio of the magma, which requires the presence of low-Cl/K end-members in the source of *F-4*.

6.2. "Zircon effect": Hf isotopic evidence

6.2.1. Hf–Nd decoupling—evidence for detritus-rich sediments in the source

Zircon $\varepsilon_{Hf}(t)$ values dramatically rise from *F-2* (mean = −10.3) to *F-4* (mean = +1.2) while whole-rock $\varepsilon_{Nd}(t)$ values vary little from *F-2* (−3.89 to −4.28) to *F-4* (−3.03 to −4.17). It seems that there exists a component in the source which controls the Lu–Hf isotopic system but has little effect on the Sm–Nd isotopic system. The Nd and Hf isotopes are nearly coupled ($\varepsilon_{Nd}(t)$ slightly lower) in *F-4* but obviously decoupled in *F-2*. Similarly, the two-stage Nd model ages are fairly similar from *F-2* to *F-4* (1.3–1.2 Ga), close to the two-stage Hf model ages of *F-4* (ca. 1.2 Ga), while totally different from the two-stage Hf model ages of *F-2* (ca. 1.8 Ga). The Hf–Nd decoupling of *F-2* results from the rather low $\varepsilon_{Hf}(t)$. Large Hf isotopic deviation might be a result of involvement of detritus-rich sediments in the source, which contain considerable amounts of detrital zircons, i.e., the sediments incorporated in the source should have a large proportion of continental detritus. Early studies questioned the possibility of presence of zircon in the sediments that subducted into the mantle. Patchett et al. (1984) considered the mixing of turbidites and pelagic sediments to be unlikely, because they might be deposited far from one another in the ocean. Thus they concluded that detrital zircons could not be transported to the abyssal plains and would not be involved in subduction-related recycling. However, Plank and Langmuir (1998) argued that Patchett's conclusion was based on the distribution of surface sediments, where there were indeed great distances between different sedimentary provinces. Plate movement produces total sedimentary columns that have Lu–Hf parameters similar to terrigenous sediments (Plank and Langmuir, 1998). Recently, "zircon effect" has been clearly observed in chemical and Hf isotopic compositions of Lesser Antilles forearc sediments (Carpentier et al., 2009). In fact, models that neglect the direct incorporation of zircon-rich detritus in the source cannot render the striking Hf–Nd decoupling in the volcanic rocks from *F-2*. Delamination of lower crust would introduce crustal material that is expected to change Hf and Nd isotopes simultaneously in the melt. Especially, garnet in the lower crust, which is enriched in Lu, might even potentially elevate $^{176}Hf/^{177}Hf$ relative to $^{143}Nd/^{144}Nd$ in the melt (Patchett et al., 1981; Schmitz et al., 2004), rather than the lowered $^{176}Hf/^{177}Hf$ observed in *F-2*. The melting of fluid-metasomatized mantle, as suggested by Liu et al. (2002), should produce magma that displays no appreciable Hf isotopic deviation from depleted mantle because Hf behaves as an immobile element in fluids (Barry et al., 2006).

6.2.2. The consumption of sediments in the source from F-2 to F-4

The variation of $\varepsilon_{Hf}(t)$ values from *F-2* to *F-4* reflects the varied amount of detritus-rich sediments incorporated into the source. $\varepsilon_{Hf}(t)$ values rise significantly from *F-2* to *F-4*, indicating that the detritus-rich sediments were gradually consumed relative to other end-members in the source. This speculation is supported by a comparative study of LILEs of the three formations. We index incompatible elements to Nb, which is both conservative and highly incompatible, and plot these ratios against Nb, to distinguish between source variation and fractional crystallization during magma ascending.

Fig. 13 shows that Rb/Nb, Ba/Nb, K/Nb, Sr/Nb and La/Nb form remarkable decreasing trends with increasing Nb. Assuming that trace element concentrations satisfy the fractional crystallization equation:

$$\frac{C'_\alpha}{C_\alpha} = F^{D_\alpha - 1} \quad (1)$$

$$\frac{C'_\beta}{C_\beta} = F^{D_\beta - 1} \quad (2)$$

whereby C_α and C_β = concentrations of element α and β in the parental magma respectively, C'_α and C'_β = concentrations of element

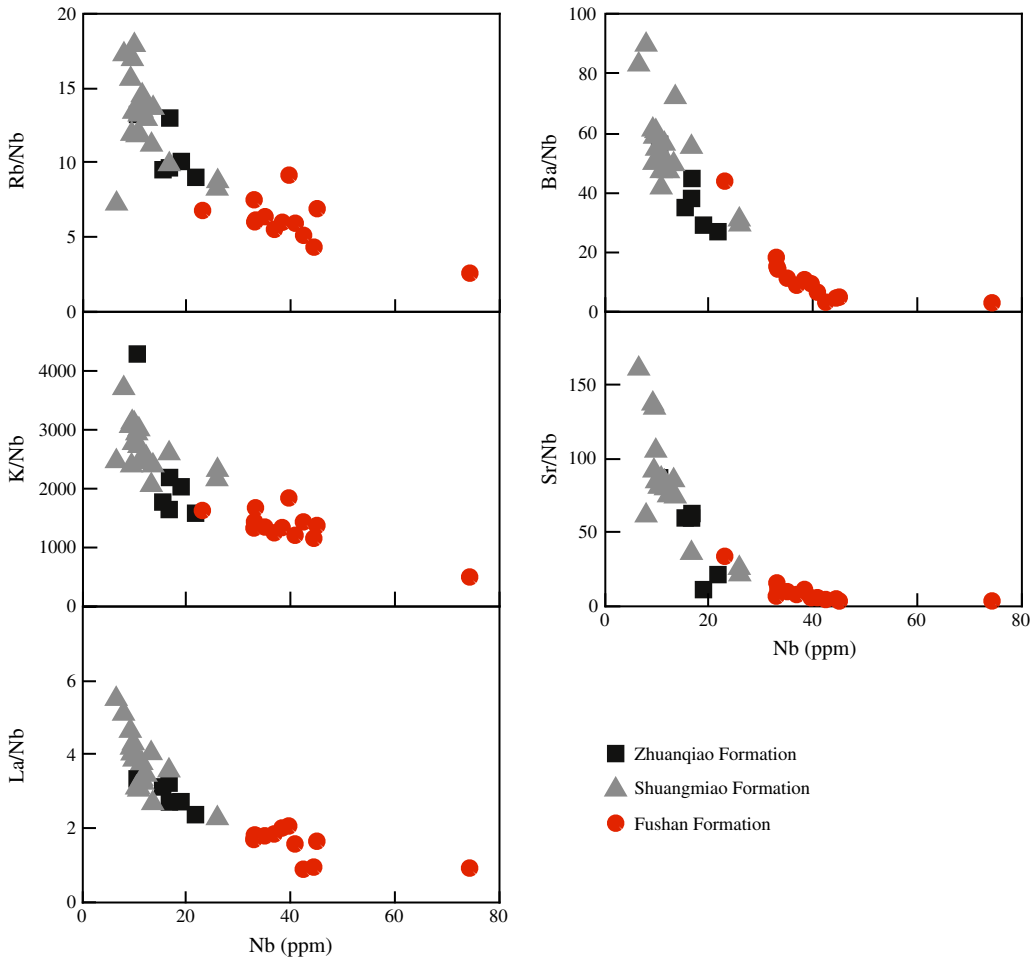

Fig. 13. Plots of Rb/Nb vs. Nb, Ba/Nb vs. Nb, K/Nb vs. Nb, Sr/Nb vs. Nb and La/Nb vs. Nb. See the negative correlation in all plots. LILE/Nb and La/Nb decrease with the increase of Nb and reaches the low-most point when it comes to the Fushan Formation. Data from Liu et al. (2002), Wang et al. (2006), Xie et al. (2007) and this study.

α and β in the upwelling melt respectively, D_α and D_β = bulk partitioning coefficients of element α and β respectively, F = crystallinity. Accordingly:

$$\frac{C'_\alpha}{C'_\beta} = \frac{C_\alpha}{C_\beta} \bullet F^{D_\alpha - D_\beta} \tag{3}$$

where F could be substituted as:

$$F = \left(\frac{C'_\beta}{C_\beta}\right)^{\frac{1}{D_\beta - 1}} \tag{4}$$

Thus, Eq. (3) could be written as:

$$\frac{C'_\alpha}{C'_\beta} = \left(\frac{C_\alpha}{C_\beta}\right) \bullet \left(\frac{C'_\beta}{C_\beta}\right)^{\frac{D_\alpha - D_\beta}{D_\beta - 1}} \tag{5}$$

The partial derivative of Eq. (5) with respect to C'_β:

$$\frac{\partial\left(\frac{C'_\alpha}{C'_\beta}\right)}{\partial C'_\beta} = \left[\left(\frac{C_\alpha}{C_\beta}\right) \bullet \left(\frac{D_\alpha - D_\beta}{D_\beta - 1}\right) \bullet C_\beta^{\frac{D_\beta - D_\alpha}{D_\beta - 1}}\right] \bullet C'_\alpha{}^{\frac{1 + D_\alpha - 2D_\beta}{D_\beta - 1}} \tag{6}$$

A more incompatible element corresponds to a smaller D. Suppose that element α is more incompatible than element β, and we find the right side of Eq. (6) > 0. With the left side of Eq. (6) symbolizing the slope of the trend plotted in α/β vs. β, we expect a positive correlation between α/β and β. On the contrary, when element α is less incompatible than element β, a negative correlation should be expected.

Generally, Rb and Ba are more incompatible than Nb in magmatic system while K, Sr less incompatible. Therefore, a positive correlation between Rb/Nb vs. Nb and Ba/Nb vs. Nb is expected and a negative one for K/Nb vs. Nb and Sr/Nb vs. Nb. However, Fig. 13 shows a pronounced negative correlations between LILE/Nb ratio vs. Nb for all Rb, Ba, K and Sr. Negative correlation between Rb/Nb vs. Nb and Ba Nb vs. Nb is hard to understand for a magmatic evolution that is governed by fractional crystallization. In fact, the above modeling is based on the assumption that the source is broadly homogeneous and stays constant in composition throughout the time. Ideally, a dual-end-member source is required to produce batches of magma that render the elemental evolution observed in Fig. 13: one is characterized by relative LILE (and probably LREE) enrichment while the other is characterized by relative Nb enrichment. Higher Nb content in whole rock requires more Nb-rich end-member added to the source, thus yielding lower LILE/Nb ratios as observed. The younger *F-4* trachytes has the lowest Rb/Nb, Ba/Nb, K/Nb and Sr/Nb ratios, suggesting that the LILE-rich end-member accounts for a remarkably smaller proportion in the source of *F-4*. Similarly, La/Nb ratio drops significantly from *F-2* and *F-3* (~5) to *F-4* (~1.5), indicating less addition of supracrustal materials into the magma source for *F-4*. As suggested above, there are four possible end-members in the source of the Luzong volcanic rocks: dehydrated sediments, dehydrated

altered oceanic crust, dehydrated unaltered oceanic crust and depleted mantle. Dehydrated sediments and/or altered oceanic crust act as the LILE-rich end-member(s) while unaltered oceanic crust and/or depleted mantle act as the relative Nb-rich end-member(s). Sediments are gradually consumed relative to the other three end-members from *F-2* to *F-4*, making altered oceanic crust the dominant contributor for the excess LILEs of *F-4*. Exactly, the source of *F-4* might be mostly composed of altered/unaltered oceanic crust, depleted mantle and the residual products (crust- and mantle-derived) of the previous partial melting batches.

6.3. Timing of the subduction event

Though the Lu–Hf isotopes obtained from zircons from the Luzong volcanic rocks represent mixing isotopic compositions of four end-members, these four end-members played quite different roles in producing the Hf isotopic compositions in the source. Depleted mantle contributed little to the Hf isotopic compositions of the source for two reasons below:

(1) The Luzong volcanic rocks are characteristic of rather low Cr and Ni contents (less than 10 ppm, generally), both of which are quite abundant in depleted mantle (Cr ~ 2500 ppm, Ni ~ 1960 ppm; Salters and Stracke, 2004) but relatively low in oceanic crust (Cr ~ 270 ppm, Ni ~ 135 ppm; Taylor et al. 1985) and GLOSS (Cr ~ 78.9 ppm, Ni ~ 70.5 ppm; Plank and Langmuir, 1998). Though Cr and Ni are gradually consumed during fractional crystallization, it will still be puzzling to observe the whole-rock Ni and Cr concentrations as low as low-Ca granite (Cr ~ 4.1 ppm, Ni ~ 4.5 ppm; Turekian and Wedepohl, 1961) while whole-rock compositions stay basaltic or trachytic. One possible explanation is that the materials derived from depleted mantle had very limited contribution to the source of the Luzong volcanic rocks.

(2) Abundances of trace elements, including Hf, are extremely low in depleted mantle, less than those of oceanic crust and sediments by a magnitude or more. For example, an ideal source consists of 70% from depleted mantle and 20% from oceanic crust as well as 10% from detrital sediments (all in wt.%) receives less than 20% Hf from depleted mantle. Therefore, low Hf content makes depleted mantle rather inefficient in controlling the source Hf isotopic compositions in the presence of oceanic crust and sediments.

Since altered and unaltered oceanic crust have similar Lu–Hf isotopes, zircon two-stage Hf model ages of the Luzong volcanic rocks are actually controlled by two end-members: detritus-rich sediments and the subducted oceanic crust. "Zircon effect" is remarkable in *F-2*, making the calculated zircon Hf T_{DM2} of *F-2* significantly older than the actual age of the oceanic crust. Whereas, detrital sediments gradually faded away from *F-2* to *F-4* and two-stage Hf model ages of *F-4* (ca. 1.2 Ga) are fairly consistent with the two-stage Nd model ages (1.3–1.2 Ga). Approximately coupled Hf–Nd model ages indicate that the source of *F-4* receives the least contribution from detritus-rich sediments. Thus, the two-stage Hf and Nd model ages of *F-4* provide a relatively close proxy for the formation age of the oceanic crust. It goes, therefore, the subducted oceanic crust might be around 1.2 Ga old, and the subduction process should take place at ca. 1.0 Ga, which is absolutely older than the formation time of the Luzong volcanic rocks.

The subducted Paleo-Pacific plate has been favored by quite a lot of researchers as the material source (or an end-member) when they explained the large-scale Mesozoic magmatic events that took place in eastern China, including the Luzong area (e.g., John et al., 1990; Faure and Natal'in, 1992; Lapierre et al., 1997; Li and Zhou, 1999; Li, 2000; Liu et al., 2002; Li and Li, 2007). However, modern oceanic crust is hardly older than 200 Ma, and thus the Paleo-Pacific oceanic crust that subducted in the Mesozoic is unlikely to be much older than 400 Ma, suggesting that the Mesozoic Pacific plate subduction model is an impossible material source for the generation of the Luzong volcanic rocks.

In fact, the Neoproterozoic magmatism and the related subduction processes are very significant in South China, especially in the periphery of the Yangtze Block. According to the tectonic location of the Luzong volcanic rocks, two possible early Neoproterozoic subduction zones can be responsible for the oceanic crust and sediments in the formation of these volcanic rocks: one in the northern margin of the Yangtze Block, and the other in the southeastern margin of the Yangtze Block. The former area consists of a great amount of Neoproterozoic granitic and basaltic rocks that were finally metamorphosed to form the UHP metamorphic rocks in the Sulu-Dabie Orogen during the Triassic continent–continent collision (Li et al., 1993) between the South and North China blocks, while the latter shows a clear arc–continent collision history that led to the formation of the Jiangnan orogen at ca. 860–800 Ma (Wang et al., 2007). We think the subduction in the northern margin of the Yangtze Block may not be responsible here, because the Luzong area could not have been so close to the north margin of the Yangtze Block at that time, or it will be difficult to imagine that the subducted oceanic crust and related sediments could be preserved so well in the lithospheric mantle and survived later Triassic intense tectonic events that included continental deep subduction and significant

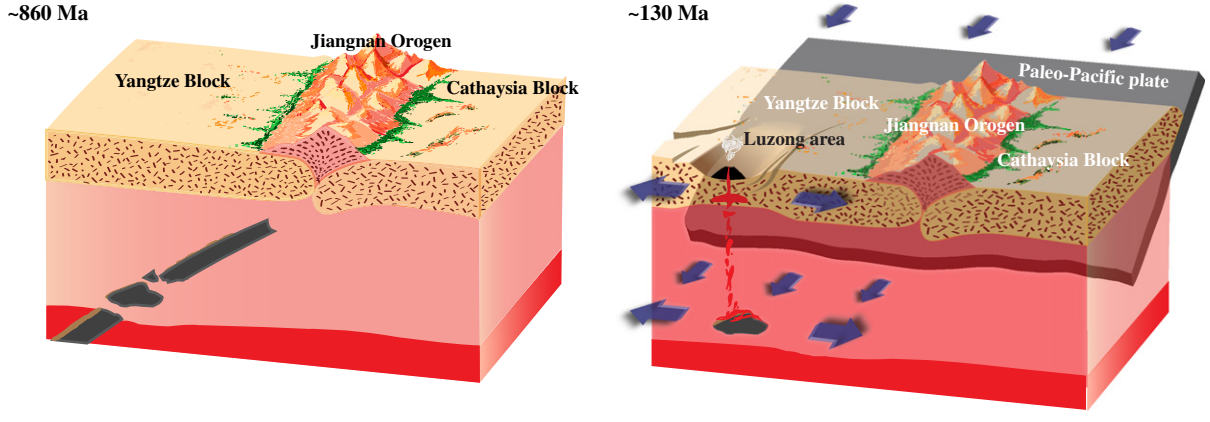

Fig. 14. Cartoons illustrating the genesis of the late Mesozoic Luzong volcanic rocks. Slab fragments of the ancient ocean between the Yangtze and Cathaysia Block that closed up at ~860 Ma, were retained in the upper mantle till back-arc extention gave rise to their partial melting in the late Mesozoic.

exhumation. Moreover, there is strong rift magmatism along the north margin of the Yangtze Block in the Neoproterozoic (Zheng et al., 2004), which is hardly seen in or near the Luzong area. Strong mantle convection, as the trigger mechanism of rift magmatism, might have also seriously endangered the preservation of the slab fragments and sediments blocked in the nearby mantle.

On the other hand, however, the Jiangnan Orogen has remained stable since its formation, with few weak interferences, e.g., Paleozoic and earlier Mesozoic activities. The early subduction process in the area is supported by the Neoproterozoic ophiolites (Zhou et al., 1989; Chen, et al., 1991; Li and McCulloch, 1996) and arc volcanic rocks in the eastern Jiangnan orogen (Li et al., 2009). Moreover, it has been proposed that the juvenile crust growth took place in late Mesoproterozoic to early Neoproterozoic (Zheng et al., 2008), with the model Hf–Nd model ages ranges from 1.3 to 1.2 Ga, similar to those of the Luzong volcanic rocks. Therefore, the early Neoproterozoic subduction to the eastern margin of the Yangtze Block might bring some materials (including the oceanic crust and overlain sediments) to the deeper part which became the source for the later formation of Luzong volcanic rocks.

The scenario could now be described as follows: ~200 km lateral subduction brought the slab and sediments through the sub-arc regime and probably down to the keel of the lithospheric mantle beneath the Yangtze Block. The early-stage subduction had efficiently extracted Cl and part of the water buried in the slab and the sediments above. The slab then broke down into fragments in the mantle during deep subduction. Given their slightly higher density, a few of the small-size slab fragments might still be blocked in the rigid lithospheric mantle and stopped subducting. These slab fragments were retained in the upper mantle for a long time until the late Mesozoic, when the west and northwest subduction of the Paleo-Pacific plate produced back-arc extentional settings (Xu et al., 2010). Lithospheric extension triggered the decompression melting of the ancient slab fragments and sediments retained in the upper mantle as well as depleted mantle beneath the Luzong area in the late Mesozoic, and resulted in the formation of the Luzong Basin (Fig. 14).

7. Conclusions

We conclude that the late Mesozoic Luzong volcanic rocks originated from partial melting of Neoproterozoic oceanic crust and overlain sediments as well as depleted lithospheric mantle. Contrasting low-Cl apatites and high-K whole rocks indicate the strong Cl–K decoupling of the primitive magma, which requires the existence of highly dehydrated (detritus-rich) sediments and dehydrated altered oceanic crust in the source. Presence of detritus-rich sediments in the source is supported by the observed “zircon effect”. Coupled Hf–Nd model ages of the younger Fushan Formation imply that the subduction responsible for the oceanic crust and sediments might take place in the early Neoproterozoic era.

Apatite, a ubiquitous mineral in igneous rocks, could provide a precious tool to learn the halogen composition of melt, especially for old rocks when melt inclusions are unavailable. More attention should be paid to the Cl-poor apatite from K-rich volcanic rocks, which may imply the strong Cl–K decoupling in the primitive magma. Extremely low Cl/K ratio might prove to be a powerful indicator of highly dehydrated subducted materials preserved in the deep lithospheric mantle for intraplate magmatism.

Supplementary materials related to this article can be foundonline at doi:10.1016/j.gr.2011.05.009.

Acknowledgments

This work was financially supported by the National Natural Science Foundation of China (grant nos. 40730313 and 40802017) and the State Key Laboratory of Mineral Deposit Research, NJU (grant no. 2008-III-01, 02). We thank J. Yan for field work assistance, H.J. Gong (NWU) for CL imaging, W.L. Zhang for apatite EMP analysis, B. Wu for LA-ICP-MS zircon U–Pb dating, and M.Y. Dai for LA-MC-ICP-MS zircon Hf isotope analysis.

References

Aiuppa, A., Federico, C., Giudice, G., Gurrieri, S., Paonita, A., Valenza, M., 2004. Plume chemistry provides insights into mechanisms of sulfur and halogen degassing in basaltic volcanoes. Earth and Planetary Science Letters 222, 469–483.
Andersen, T., 2002. Correction of common lead in U–Pb analyses that do not report ^{204}Pb. Chemical Geology 192, 59–79.
Aoki, K., Ishiwaka, K., Kanisawa, S., 1981. Fluorine geochemistry of basaltic rocks from continental and oceanic regions and petrogenetic application. Contributions to Mineralogy and Petrology 76, 53–59.
Barry, T.L., Pearce, J.A., Leat, P.T., Millar, I.L., Roex, A.P.L., 2006. Hf isotope evidence for selective mobility of high-field-strength elements in a subduction setting: South Sandwich Islands. Earth and Planetary Science Letters 252, 223–244.
Black, L.P., Gulson, B.L., 1978. The age of the Mud Tank carbonatite, Strangways Range, Northern Territory. BMR Journal of Australian Geology and Geophysics 3, 227–232.
Blichert-Toft, J., Albarede, F., 1997. The Lu–Hf geochemistry of chondrites and the evolution of the mantle–crust system. Earth and Planetary Science Letters 148, 243–258.
Boudreau, A.E., McCallum, I.S., 1989. Investigation of the Stillwater Complex: Part V. Apatites as indicators of evolving fluid composition. Contributions to Mineralogy and Petrology 102, 138–153.
Boudreau, A.E., Love, C., Prendergast, M.D., 1995. Halogen geochemistry of the Great Dyke, Zimbabwe. Contributions to Mineralogy and Petrology 122, 289–300.
Boyce, J.W., Hervig, R.L., 2009. Apatite as a monitor of late-stage magmatic processes at Volcán Irazú, Costa Rica. Contributions to Mineralogy and Petrology 157, 135–145.
Brearly, A.J., Jones, R.H., 1998. Chondritic meteorites. In: Papike, J.J. (Ed.), Planetary Materials. Reviews in Mineralogy, vol. 36. Mineralogical Society of America, Washington, DC, pp. 3.1–3.398.
Brehler, B., Fuge, R., 1974. Chlorine. In: Wedepohl, K.H. (Ed.), Handbook of Geochemistry, Vol. II-2. 17A-17O.
Brenan, J., 1993. Partitioning of fluorine and chlorine between apatite and aqueous fluids at high pressure and temperature: implications for the F and Cl content of high P–T fluids. Earth and Planetary Science Letters 117, 251–263.
Busigney, V., Cartigny, P., Philippot, P., Ader, M., Javoy, M., 2003. Massive recycling of nitrogen and other fluid-mobile elements (K, Rb, Cs, H) in a cold slab environment: evidence from HP to UHP oceanic sediments of the Schistes Lustre nappe (western Alps, Europe). Earth and Planetary Science Letters 215, 27–42.
Carpentier, M., Chauvel, C., Maury, R.C., Mattielli, N., 2009. The “zircon effect” as recorded by the chemical and Hf isotopic compositions of Lesser Antilles forearc sediments. Earth and Planetary Science Letters 287, 86–99.
Chen, J.F., Foland, K.A., Xing, F.M., Xu, X., Zhou, T.X., 1991. Magmatism along the southeast margin of the Yangtze block: Precambrian collision of the Yangtze and Cathaysia blocks of China. Geology 19, 815–818.
Chu, N.C., Taylor, R.N., Chavagnac, V., Nesbitt, R.W., Boella, R.M., Milton, J.A., Germain, C.R., Bayon, G., Burton, K., 2002. Hf isotope ratio analysis using multi-collector inductively coupled plasma mass spectrometry: An evaluation of isobaric interference corrections. Journal of Analytical Atomic Spectrometry 17, 1567–1574.
Davis, M.G., Garcia, M.O., Wallace, P., 2003. Volatiles in glasses from Mauna Loa Volcano, Hawai'i: implications for magma degassing and contamination and growth of Hawaiian volcanoes. Contribution to Mineralogy and Petrology 144, 570–591.
Douce, A.E.P., Roden, M., 2006. Apatite as a probe of halogen and water fugacities in the terrestrial planets. Geochimica et Cosmochimica Acta 70, 3173–3196.
Drake, M.J., Weill, D.F., 1975. Partition of Sr, Ba, Ca, Y, Eu^{2+}, Eu^{3+}, and other REE between plagioclase feldspar and magmatic liquid: an experimental study. Geochimica et Cosmochimica Acta 39, 689–712.
Dungan, M.A., Lindstrom, M.M., McMillan, N.J., Moorbath, S., Hoefs, J., Haskin, L., 1986. Open system magmatic evolution of the Taos Plateau volcanic field, northern New Mexico I: the petrology and geochemistry of the Servilleta Basalt. Journal of Geophysical Research 91, 5999–6028.
Fan, W.M., Zhang, H.F., Baker, J., Jarvis, K.E., Mason, P.R.D., Menzies, M.A., 2000. On and off the North China craton: where is the Archaean keel? Journal of Petrology 41, 933–950.
Faure, M., Natal'in, 1992. The geodynamic evolution of the eastern Eurasian margin in Mesozoic times. Tectonophysics 208, 397–411.
Fodor, R.V., 2001. The role of tonalite and diorite in Mauna Kea volcano, Hawaii, magmatism: petrology of summit-region leucocratic xenoliths. Journal of Petrology 42, 1685–1704.
Folco, L., Bland, P.A., D'Orazio, M., Franchi, I.A., Kelley, S.P., Rocchi, S., 2004. Extensive impact melting on the H-chondrite parent asteroid during cataclysmic bombardment of the early solar system: Evidence from the achondritic meteorite Dar al Gani 896. Geochimica et Cosmochimica Acta 68, 2379–2397.
Griffin, W.L., Pearson, N.J., Elusive, E., Jackson, S.E., van Achtenberg, E., O'Reilly, S.Y., She, S.R., 2000. The Hf isotope composition of carbonic mantle: LAM-MC-ICPMS analysis of zircon megacrysts in kimberlites. Geochimica et Cosmochimica Acta 64, 133–147.
Griffin, W.L., Wang, X., Jackson, S.E., Pearson, S.E., O'Reilly, S.Y., Xu, X.S., Zhou, X.M., 2002. Zircon chemistry and magma genesis, SE China: in-situ analysis of Hf isotopes, Tonglu and Pingtan Igneous Complexes. Lithos 61, 237–269.

Hansteen, T.H., Gurenko, A.A., 1998. Sulfur, chlorine, and fluorine in glass inclusions in olivine and clinopyroxene from basaltic hyaloclastites representing the Gran Canaria Shield Stage at Sites 953 and 956. In: Weaver, P.P.E., Schmincke, H.-U., Firth, J.V., Duffield, W. (Eds.), Proceedings of the Ocean Drilling Program, Scientific Results, Vol. 157, pp. 403–410.
Hermann, J., 2002. Allanite: thorium and light rare earth element carrier in subducted crust. Chemical Geology 192, 289–306.
Hermann, J., Green, D.H., 2001. Experimental constraints on high pressure melting in subducted crust. Earth and Planetary Science Letters 188, 149–168.
Hermann, J., Rubatto, D., 2009. Accessory phase control on the trace element signature of sediment melts in subduction zones. Chemical Geology 265, 512–526.
Huntington, H.D., 1979. Kiglapait mineralogy I: apatite, biotite and volatiles. Journal of Petrology 20, 625–652.
Iizuka, T., Hirata, T., 2005. Improvements of precision and accuracy in in situ Hf isotope microanalysis of zircon using the laser ablation-MC-ICPMS technique. Chemicl Geology 220, 121–137.
Jackson, S.E., Pearson, N.J., Griffin, W.L., Belousova, E.A., 2004. The application of laser ablation-inductively coupled plasma-mass spectrometry to in situ U–Pb zircon geochronology. Chemical Geology 211, 47–69.
Jambon, A., Deruelle, B., Dreibus, G., Pineau, F., 1995. Chlorine and bromine abundance in MORB: the contrasting behavior of the Mid-Atlantic Ridge and East Pacific Rise and implications for chlorine geodynamic cycle. Chemical Geology 126, 101–117.
John, B.M., Zhou, X.H., Li, J.L., 1990. Formation and tectonic evolution of southeastern China and Taiwan: isotopic and geochemical constraints. Tectonophys 183, 145–160.
Kelley, K.A., Plank, T., Ludden, J., Staudigel, H., 2003. Composition of altered oceanic crust at ODP Sites 801 and 1149. Geochemistry Geophysics Geosystem 4. doi:10.1029/2002GC000435. Paper number: 2002GC000435.
Kurat, G., Zinner, E., Brandstätter, F., 2002. A plagioclase–olivine–spinel–magnetite inclusion from Maralinga (CK): evidence for sequential condensation and solid-gas exchange. Geochimica et Cosmochimica Acta 66, 2959–2979.
Lapierre, H., John, B.M., Charvet, J., Yu, Y.W., 1997. Mesozoic felsic arc magmatism and continental olivine tholeiites in Zhejiang Province and their relationship with the tectonic activity in southeastern China. Tectonophysics 274, 321–338.
Lassiter, J.C., Hauri, E.H., Nikogosian, I.K., Barsczus, H.G., 2002. Chlorine–potassium variations in melt inclusions from Raivavae and Rapa, Austral Islands: Constraints on chlorine recycling in the mantle and evidence for brine-induced melting of oceanic crust. Earth and Planetary Science Letters 202, 525–540.
Li, X.H., 2000. Cretaceous magmatism and lithospheric extension in Southeast China. Journal of Asian Earth Sciences 18, 293–305.
Li, Z.X., Li, X.H., 2007. Formation of the 1300 km-wide intra-continental orogen and post-orogenic magmatic province in Mesozoic South China: A flat-slab subduction model. Geology 35, 179–182.
Li, X.H., McCulloch, M.T., 1996. Secular variation in the Nd isotopic composition of Neoproterozoic sediments from the southern margin of the Yangtze Block: Evidence for a Proterozoic continental collision in southeast China. Precambrian Research 76, 67–76.
Li, Y.H., Schoomaker, J.E., 2003. Chemical composition and mineralogy of marine sediments. In: Holland, H.D., Turekian, K.K. (Eds.), Treatise on geochemistry, Vol. 7, pp. 1–35.
Li, W.X., Zhou, X.M., 1999. Late Mesozoic subduction zone of southeastern China. Geological Journal of China Universities 5, 164–168 (in Chinese with English abstract).
Li, S.G., Xiao, Y., Liou, D., Chen, Y.Z., Ge, N.J., Zhang, Z.Q., Sun, S.S., Cong, B., Zhang, R.Y., Hart, S.R., Wang, S.H., 1993. Collision of the North China and Yangtze blocks and formation of coesite-bearing eclogites, timing and processes. Chemical Geology 109, 89–111.
Li, X.H., Li, W.X., Li, Z.X., Lo, Q.H., Wang, J., Ye, M.F., Yang, Y.H., 2009. Amalgamation between the Yangtze and Cathaysia Blocks in South China: Constraints from SHRIMP U–Pb zircon ages, geochemistry and Nd–Hf isotopes of the Shuangxiwu volcanic rocks. Precambrian Research 174, 117–128.
Liu, H., Qiu, J.S., Luo, Q.H., Xu, X.S., Ling, W.L., Wang, D.Z., 2002. Petrogenesis of the Mesozoic potash-rich volcanic rocks in the Luzong basin, Anhui Province: Geochemical constraints. Geochemica 31, 129–140 (in Chinese with English abstract).
Ludwig, K.R., 1999. User's Manual for Isoplot/Ex Version 2.06: A Geochronological Toolkit for Microsoft Excel, vol. 1a (Special Publication). Geochronology Center, Berkeley, pp. 1–49.
Lyubetskaya, T., Korenaga, J., 2007. Chemical composition of Earth's primitive mantle and its variance: 1. Method and results. Journal of Geophysical Research 112, B03211.
Machado, N., Simonetti, A., 2001. U–Pb dating and Hf isotopic composition of zircons by laser ablation-MC-ICP-MS. In: Sylvester, P. (Ed.), Laser-ablation-ICPMS in the Earth Sciences: Principles and Applications, 29. Short Course of Mineralogical Association of Canada, pp. 121–146.
McCoy, T.J., Keil, K., Clayton, R.N., Mayeda, T.K., Bogard, D.D., Garrison, D.H., Huss, G.R., Hutcheon, I.D., Wieler, R., 1996. A petrologic, chemical, and isotopic study of Monument Draw and comparison with other acapulcoites: Evidence for formation by incipient partial melting. Geochimica et Cosmochimica Acta 60, 2681–2708.
McHone, J.G., 2002. Volatile emissions from Central Atlantic Magmatic Province basalts: Mass assumptions and environmental consequences. Geophysical Monograph 136, 241–254.
Meurer, W.P., Natland, J.H., 2001. Apatite compositions from oceanic cumulates with implications for the evolution of mid-ocean ridge magmatic systems. Journal of Volcanology and Geothermal Research 110, 281–298.
Michael, P.J., Cornell, W.C., 1998. Influence of spreading rate and magma supply on crystallization and assimilation beneath mid-ocean ridges: Evidence from chlorine and major element chemistry of mid-ocean ridge basalts. Journal of Geophysical Research 103, 18325–18356.
Min, K., Farley, K.A., Renne, P.R., Marti, K., 2003. Single grain (U–Th)/ He ages from phosphates in Acapulco meteorite and implications for thermal history. Earth and Planetary Science Letters 209, 323–336.
Moune, S., Sigmarsson, O., Thordarson, T., Gauthier, P.J., 2007. Recent volatile evolution in the magmatic system of Hekla volcano, Iceland. Earth and Planetary Science Letters 255, 373–389.
Nash, W.P., 1976. Fluorine, chlorine and OH-bearing minerals in the Skaergard intrusion. American Journal of Science 276, 546–557.
Nowell, G.M., Kempton, P.D., Noble, S.R., Fitton, J.G., Saunders, A.D., Mahoney, J.J., Taylor, R.N., 1998. High precision Hf isotope measurements of MORB and OIB by thermal ionisation mass spectrometry: Insights into the depleted mantle. Chemical Geology 149, 211–233.
O'Reilly, S.Y., Griffin, W.L., 2000. Apatite in the mantle: Implication for metasomatic processes and high heat production in Phanerozoic mantle. Lithos 53, 217–232.
Ono, S., 1998. Stability limits of hydrous minerals in sediment and mid-ocean ridge basalt compositions: implications for water transport in subduction zones. Journal of Geophysical Research 103, 18253–18267.
Patchett, P.J., Kouvo, O., Hedge, C.E., Tatsumoto, M., 1981. Evolution of continental crust and mantle heterogeneity: evidence from Hf isotopes. Contributions to Mineralogy and Petrology 78, 279–297.
Patchett, P.J., White, W.M., Feldmann, H., Kielinczuk, S., Hofmann, A.W., 1984. Hafnium/rare earth element fractionation in the sedimentary system and crustal recycling into the Earth's mantle. Earth and Planetary Science Letters 69, 365–378.
Peng, G., Luhr, J.F., McGee, J.J., 1997. Factors controlling sulfur concentrations in volcanic apatites. American Mineralogist 82, 1210–1224.
Piccoli, P.M., Candela, P.A., 2002. Apatite in igneous systems. Reviews in Mineralogy and Geochemistry 48, 255–292.
Plank, T., Langmuir, C.H., 1998. The chemical composition of subducting sediment and its consequences for the crust and mantle. Chemical Geology 145, 323–394.
Prowatke, S., Klemme, S., 2006. Trace element partitioning between apatite and silicate melts. Geochimica et Cosmochimica Acta 70, 4513–4527.
Pu, W., Gao, J.F., Zhao, K.D., Ling, H.F., Jiang, S.Y., 2005. Separation method of Rb–Sr, Sm–Nd using DCTA and HIBA. Journal of Nanjing University (Natural Science) 41, 445–450.
Pyle, D.M., Mather, T.A., 2009. Halogens in igneous processes and their fluxes to the atmosphere and oceans from volcanic activity: A review. Chemical Geology 263, 110–121.
Rapp, R.P., Irifune, T., Shimizu, N., Nishiyama, N., Norman, M.D., Inoue, T., 2008. Subduction recycling of continental sediments and the origin of geochemically enriched reservoirs in the deep mantle. Earth and Planetary Science Letters 271, 14–23.
Rowe, M.C., Lassiter, J.C., 2009. Chlorine enrichment in central Rio Grande Rift basaltic melt inclusions: Evidence for subduction modification of the lithospheric mantle. Geology 37, 439–442.
Rudnick, R.L., Gao, S., 2004. Composition of the continental crust. In: Holland, H.D., Turekian, K.K. (Eds.), Treatise on geochemistry, Vol. 3, pp. 1–64.
Salters, V.J.M., Stracke, A., 2004. Composition of the depleted mantle. Geochemistry Geophysics Geosystem 5. doi:10.1029/2003GC000597. Paper number: 2003GCOOO597.
Scambelluri, M., Müntener, O., Ottolini, L., Pettke, T.T., Vannucci, R., 2004. The fate of B, Cl and Li in the subducted oceanic mantle and in the antigorite breakdown fluids. Earth and Planetary Science Letters 222, 217–234.
Scherer, E., Munker, C., Mezger, K., 2001. Calibration of the lutetium–hafnium clock. Science 293, 683–687.
Schilling, J.G., Bergeron, M.B., Evans, R., 1980. Halogens in the mantle beneath the North Atlantic. Philosophical Transactions of the Royal Society of London A297, 147–178.
Schmidt, M.W., 1996. Experimental constraints on recycling of potassium from subducted oceanic crust. Science 272, 1927–1930.
Schmitz, M.D., Vervoot, J.D., Bowring, S.A., Patchett, P.J., 2004. Decoupling of the Lu–Hf and Sm–Nd isotope system during the evolution of granulitic lower crust beneath southern Africa. Geology 32, 405–408.
Semenenko, V.P., Girich, A.L., Nittler, L.R., 2004. An exotic kind of cosmic material: Graphite-containing xenoliths from the Krymka (LL31) chondrite. Geochimica et Cosmochimica Acta 68, 455–475.
Sha, L.K., Chappell, B.W., 1999. Apatite chemical composition, determined by electron microprobe and laser-ablation inductively coupled plasma mass spectrometry, as a probe into granite petrogenesis. Geochimica et Cosmochimica Acta 63, 3861–3881.
Shao, J.A., Liu, F.T., Chen, H., 2000. Seismic tomography profile of Northwest Pacific and its implication for the Earth dynamics. Progress in Natural Science 10, 757–761 (in Chinese).
Sigvaldason, G.E., Óskarsson, N., 1986. Fluorine in basalts from Iceland. Contributions to Mineralogy and Petrology 94, 263–271.
Spandler, C., Hermann, J., Arculus, R., Mavrogenes, J., 2003. Redistribution of trace elements during prograde metamorphism from lawsonite blueschist to eclogite facies; implications for deep subduction-zone processes. Contributions to Mineralogy and Petrology 146, 205–222.
Spengler, S.R., Garcia, M.O., 1988. Geochemistry of the Hawi lavas, Kohala Volcano, Hawaii. Contributions to Mineralogy and Petrology 99, 90–144.
Stelling, J., Botcharnikov, R.E., Beermann, O., Nowak, M., 2008. Solubility of H2O- and Chlorine-bearing fluids in basaltic melt of Mount Etna at T = 1050–1250 °C and P = 200 MPa. Chemical Geology 256, 101–109.
Stern, C.R., 2011. Subduction erosion: Rates, mechanisms, and its role in arc magmatism and the evolution of the continental crust and mantle. Gondwana Research. doi:10.1016/j.gr.2011.03.006.
Straub, S.M., Layne, G.D., 2003a. Decoupling of fluids and fluid-mobile elements during shallow subduction: Evidence from halogen-rich andesite melt inclusions from the

Izu arc volcanic front. Geochemistry Geophysics Geosystem 4. doi:10.1029/2002GC000349. Paper number: 2002GC000349.
Straub, S.M., Layne, G.D., 2003b. The systematics of chlorine, fluorine, and water in Izu arc front volcanic rocks: Implications for volatile recycling in subduction zones. Geochimica et Cosmochimica Acta 67, 4179–4203.
Sun, S.S., McDonough, W.D., 1989. Chemical and isotopic systematics of oceanic basalts: implications for mantle composition and processes. In: Saunders, A.D., Norry, M.J. (Eds.), Magmatism in the Ocean Basins: Geological Society of London Special Publication, 42, pp. 313–345.
Tanaka, T., Togashi, S., Kamioka, H., Amakawa, H., Kagami, H., Hamamoto, T., Yuhara, M., Orihashi, Y., Yoneda, S., Shimizu, H., Kunimaru, T., Takahashi, K., Yanagi, T., Nakano, T., Fujimaki, H., Shinjo, R., Asahara, Y., Tanimizu, M., Dragusanu, C., 2000. JNDi-1: a neodymium isotopic reference in consistency with LaJolla neodymium. Chemical Geology 168, 279–281.
Taylor, S.R., McLennan, S.M., 1985. The Continental Crust: Its Composition and Evolution. Blackwell, London, pp. 57–72.
Turekian, K.K., Wedepohl, K.H., 1961. Distribution of the Elements in Major Units of the Earth Crust. Geological Society of America Bulletin 72, 172–192.
Wang, Q., Wyman, D.A., Xu, J.F., Zhao, Z.H., Jian, P., Xiong, X.L., Bao, Z.W., Li, C.F., Bai, Z.H., 2006. Petrogenesis of Cretaceous adakitic and shoshonitic igneous rocks in the Luzong area, Anhui Province (eastern China): Implications for geodynamics and Cu–Au mineralization. Lithos 89, 424–446.
Wang, X.L., Zhou, J.C., Griffin, W.L., Wang, R.C., Qiu, J.S., O'Reilly, S.Y., Xu, X.S., Liu, X.M., Zhang, G.L., 2007. Detrital zircon geochronology of Precambrian basement sequences in the Jiangnan orogen: Dating the assembly of the Yangtze and Cathaysia Blocks. Precambrian Research 159, 117–131.
Warner, S., Martin, R.F., Abdel-Rahman, A.F.M., Doig, R., 1998. Apatite as a monitor of fractionation, degassing, and metamorphism in the Sudbury Igneous Complex, Ontario. Canadian. Mineralogist 36, 981–999.
Watson, E.B., Green, T.H., 1981. Apatite/liquid partition coefficients for the rare earth elements and strontium. Earth and Planetary Science Letters 56, 405–421.
Webster, J.D., Tappen, C.M., Mandeville, C.W., 2009. Partitioning behavior of chlorine and fluorine in the system apatite-melt-fluid. II: Felsic silicate systems at 200 MPa. Geochimica et Cosmochimica Acta 73, 559–581.
Willmore, C.C., Boudreau, A.E., Kruger, F.J., 2000. The halogen geochemistry of the Bushveld Complex, Republic of South Africa: Implications for chalcophile element distribution in the Lower and Critical Zones. Journal of Petrology 41, 1517–1539.
Wolff, J.A., Rowe, M.C., Teasdale, R., Gardner, J.N., Ramos, F.C., Heikoop, C.E., 2005. Petrogenesis of pre-caldera mafic lavas, Jemez Mountains Volcanic Field (New Mexico, USZ). Journal of Petrology 46, 407–439.
Wong, J., Sun, M., Xing, G., Li, X.-H., Zhao, G.C., Wong, K., Fu, F., 2011. Zircon U–Pb and Hf isotopic study of Mesozoic felsic rocks from eastern Zhejiang, South China: Geochemical contrast between Yangtze and Cathaysia blocks. Gondwana Research 19, 244–259.
Woodhead, J., Hergt, J., Shelley, M., Eggins, S., Kemp, R., 2004. Zircon Hf-isotope analysis with an excimer laser, depth profiling, ablation of complex geometries, and concomitant age estimation. Chemical Geology 209, 121–135.
Wu, F.Y., Yang, Y.H., Xie, L.W., Yang, J.H., Xu, P., 2006. Hf isotopic compositions of the standard zircons and baddeleyites used in U–Pb geochronology. Chemical Geology 234, 105–126.
Xie, Z., Li, Q.Z., Chen, J.F., Gao, T.S., 2007. The geochemical characteristics of the early-Cretaceous volcanics in Luzong Region and Their Source Significances. Geological Journal of China Universities 13, 235–245 (in Chinese with English abstract).
Xu, X.S., Suzuki, K., Liu, L., Wang, D.Z., 2010. Petrogenesis and tectonic implications of Late Mesozoic granites in the NE Yangtze Block, China: further insights from the Jiuhuashan–Qingyang complex. Geological Magazine 147, 219–232.
Yang, J.H., O'Reilly, S., Walker, R.J., Griffin, W., Wu, F.Y., Zhang, M., Pearson, N., 2010. Diachronous decratonization of the Sino-Korean craton: geochemistry of mantle xenoliths from North Korea. Geology 38, 799–802.
Yang, S.-Y., Jiang, S.-Y., Li, L., Sun, Y., Sun, M.-Z., Bian, L.-Z., Xiong, Y.-G., Cao, Z.-Q., 2011. Late Mesozoic magmatism of the Jiurui mineralization district in the Middle-Lower Yangtze River Metallogenic Belt, Eastern China: precise U–Pb ages and geodynamic implications. Gondwana Research. doi:10.1016/j.gr.2011.03.012.
Yao, J., Shu, L., Santosh, M., 2011. Detrital zircon J–Pb geochronology, Hf-isotopes and geochemistry—new clues for the Precambrian crustal evolution of Cathaysia Block, South China. Gondwana Research. doi:10.1016/j.gr.2011.01.005.
Yuan, X.C., 2007. Mushroom structure of the lithospheric mantle and its genesis at depth: revisited. Geology in China 34, 737–758 (in Chinese with English abstract).
Yuan, H.L., Gao, S., Dai, M.N., Zong, C.L., Günther, D., Fontaine, G.H., Liu, X.M., Diwu, C.R., 2008. Simultaneous determinations of U–Pb age, Hf isotopes and trace element compositions of zircon by excimer laser-ablation quadrupole and multiple-collector ICP-MS. Chemical Geology 247, 100–118.
Zhang, Q., Qian, Q., Wang, E.Q., Wang, Y., Zhao, T.P., Hao, J., Guo, G.J., 2001. An east China plateau in mid-late Yanhanian period: Implication from adakites. Chinese Journal of Geology 36, 248–255.
Zhang, H.F., Sun, M., Zhou, X.H., Fan, W.M., Zhai, M.G., Yin, J.F., 2002. Mesozoic lithosphere destruction beneath the North China Craton: Evidence from major, trace element, and Sr–Nd–Pb isotope studies of Fangcheng basalts. Contributions to Mineralogy and Petrology 144, 241–254.
Zhang, Q., Wang, Y.L., Jin, W.J., Li, C.D., 2008. Eastern China plateau during the Late Mesozoic: Evidence, problems and implication. Geological Bulletin of China 27, 1404–1430.
Zhang, H.-F., Ying, J.-F., Tang, Y.-J., Li, X.-H., Feng, C., Santosh, M., 2011. Phanerozoic reactivation of the Archean North China Craton through episodic magmatism: evidence from zircon U–Pb geochronology and Hf isotopes from the Liaodong Peninsula. Gondwana Research 19, 446–459.
Zheng, Y.F., Wu, Y.B., Chen, F.K., Gong, B., Li, L., Zhao, Z.F., 2004. Zircon U–Pb and oxygen isotope evidence for a large-scale ^{18}O depletion event in igneous rocks during the Neoproterozoic. Geochimica et Cosmochimica Acta 68, 4145–4165.
Zheng, Y.F., Wu, R.X., Wu, Y.B., Zhang, S.B., Yuan, H.L., Wu, F.Y., 2008. Rift melting of juvenile arc-derived crust: Geochemical evidence from Neoproterozoic volcanic and granitic rocks in the Jiangnan Orogen, South China. Precambrian Research 163, 351–383.
Zhou, X.M., Zou, H.B., Yang, J.D., Wang, Y.X., 1989. Sm–Nd isochron age of ophiolites in Shexian, Anhui Province and its geological significance. Chinese Science Bulletin 34, 1243–1245 (in Chinese).
Zhou, T.F., Fan, Y., Yuan, F., Lu, S.M., Shang, S.G., Cooke, D., Meffre, S., 2008. Geochronology of the volcanic rocks from the Luzong basin and its significance. Chinese Science Bulletin 38, 1342–1353 (in Chinese).